DEGREE PROJECT IN MECHANICAL ENGINEERING,
SECOND CYCLE, 30 CREDITS
STOCKHOLM, SWEDEN 2020

IMPLEMENTATION OF MOISTURE DEPENDENT CONSTITUTIVE MODEL FOR PAPERBOARD

Master Thesis Report

VENKATA VENU SAI PHANI RAM BABBEPALLI

KTH ROYAL INSTITUTE OF TECHNOLOGY
SCHOOL OF ENGINEERING SCIENCES

ACKNOWLEDGMENTS

This thesis is submitted in partial fulfillment of the requirements for the degree of Master of Science in Engineering Mechanics at KTH Royal Institute of Technology. The work has been carried out at RISE Bioeconomy in Kista, Stockholm from January to July 2019.

First, I would like to thank Dr. Mikael Nygårds for giving me an opportunity to do my thesis at RISE. I would like to thank him for changing the thesis project to suit my interests. As one of my supervisors at RISE, he gave me the starting point and much of the material needed to proceed with the project.

I would like to thank Mr. Gustav Marin for his constant support during many times in the project. As the main supervisor at RISE, he made sure that I am on track for the thesis project and always checked on me to find out any problems I was facing. I would like to thank him especially for his constant presence, which has solved many of my administrative problems during tough times.

I would like to thank Dr. Prashanth Srinivasa, an unofficial supervisor at RISE. He made my life easy in implementing much of the stuff. I also thank him for taking out time especially for me and solving my problems. I especially would like to thank him for his support and guidance in successfully implementing the material model.

I would also like to thank Prof. Sören Östlund at KTH for his support and for guiding me in the right direction. He always made sure that the project did not drift in some other direction.

I would also like to thank Dr. Mikael Schill at Dynamore Nordic for offering me an LS DYNA course at free of cost. I would also like to thank him for the report he provided which made the implementation in LS DYNA easier.

I would also like to thank the STFIs Association of Interested Parties (STFIs Intressentförening) for the financial support of the project.

Finally, I would like to thank my mother, father, sister, and my little nephew who has given me the strength to proceed further in life. Even though they were far, they made sure that I did not lose focus or motivation.

ABSTRACT

There has been a considerable increase in the usage of paper products due to its sustainability in the product cycle. Many environmental and process variables can affect the mechanical behavior of paper from its making to finished products. Of these variables, moisture is of particular importance and strongly influences both papermaking, converting, and end-use of the paper products.

Experimental investigations at different humidity levels reveals that normalized in-plane constitutive parameters, such as elastic parameters and the linear hardening modulus, in both MD and CD[1]) follow a linear relationship with normalized moisture ratio. This relation is found to be acceptable for a wide range of commercial paperboards. To capture this observation, a novel material model with orthotropic elasticity and anisotropic hardening[2] is proposed. An associative flow rule for the evolution of plastic strain is proposed. The proposed flow rule is such that all stresses contribute to plastic flow rather than an effective stress. A simple version using anisotropic linear hardening is implemented. The mechanical properties, such as elastic parameters and hardening moduli are considered functions of the moisture ratio. An implicit variant of the material model is implemented in LS-DYNA®. The simulations with the proposed material model at different humidity levels follow the experimental results well for uniaxial loading, but discrepancies are obtained for simulation of biaxial loading tests.

The moisture is assumed constant in the proposed model since the experiments are done in a moisture-controlled environment.

[1] MD – Machine Direction; CD – Cross Direction

[2] Anisotropic Hardening – Different Hardening modulus in different directions

SAMMANFATTNING

Användningen av pappersprodukter har ökat avsevärt på grund av dess hållbarhet i produktcykeln. Många miljö- och processvariabler kan påverka papperets egenskaper från tillverkning till färdig produkt. Av dessa variabler är fukt särskilt viktig och fukt påverkar kraftigt både tillverkning, konvertering och slutanvändning av pappersprodukter.

En experimentell undersökning vid olika fuktighetsnivåer visar att normaliserade konstitutiva parametrar, såsom elastiska styvheter och tangentmodulen i papperets plan i både MD och CD, uppvisar ett linjärt samband som funktion av normaliserad fuktkvot. Detta samband har visat sig vara en god approximation för ett stort antal kommersiella kartonger. En ny materialmodell baserad på ortotrop elasticitet och anisotropt hårdnande föreslås med hänsyn till detta. En associativ flytlag för plastisk deformation föreslås. Den föreslagna flytlagen är sådan att alla spänningar bidrar till den plastiska deformationen snarare än effektivspänningen. En enklare version baserad på linjärt anisotropt hårdnande har modellerats. De mekaniska egenskaperna såsom styvhet och hårdnandemodul anses vara funktioner av fuktkvoten och följa de linjära sambanden. En implicit variant av materialmodellen är implementerad i LS-DYNA®. Simuleringar med den föreslagna materialmodellen vid olika fuktkvoter följer de experimentella resultaten väl vid enaxlig belastning medan vissa avvikelser uppträder vid tvåaxlig belastning.

I den föreslagna modellen antas fukten antas vara konstant eftersom de bakomliggande experimenten genomfördes i en fuktkontrollerad miljö.

TABLE OF CONTENTS

LIST OF FIGURES

LIST OF TABLES

LIST OF ABBREVIATIONS

MD – Machine Direction

CD – Cross Direction

ZD – Thickness Direction

FEM – Finite Element Method

UDF – User Defined Function

UMAT – User-defined Material Model

RH – Relative Humidity

1 INTRODUCTION

1.1 PAPER AS A PACKAGING MATERIAL

Paper is found almost everywhere in daily usage. Some of the products that are common and are widely used for a long time are office paper and newsprint. The earliest date of paper being used was about 2nd century BC in China (Wikipedia, n.d.). The raw product from which paper is made is pulp from wood fibers. The wood pulp is generally made from either a chemical or a mechanical process or can be a combination of both (Wikipedia, n.d.). The method of making pulp generally affects the final properties of paper.

Paper is generally considered as a 2D material because of its very low thickness. Office paper and newsprint generally have a thickness of 0.1 mm (Gustafsson & Niskanen, 2012). The thickness can be up to 1 mm in applications such as display products. Special papers can also be made with a thickness as low as 0.01 mm as well. Thick paper grades are generally termed board or paperboard.

The paper is made by spraying a suspension of water and fibers onto a moving wire, which aligns the fibers in one direction known as Machine Direction (MD). The general coordinate system used to define the paper products is shown in Figure 1.1. The other directions are defined as Cross Direction (CD) and thickness direction (ZD). Also, the x, y, z coordinate system refers to the global coordinate system.

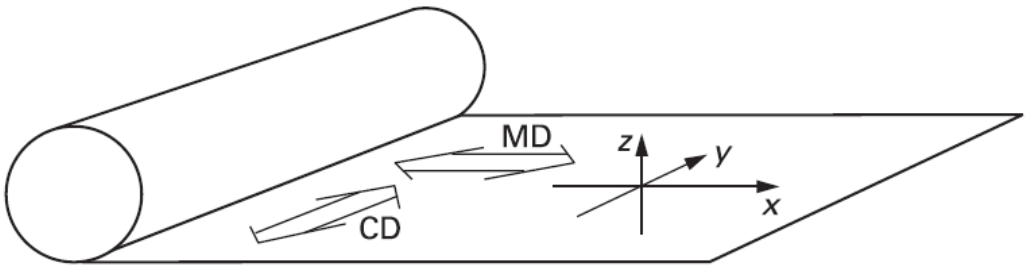

Figure 1.1 Coordinate system used for paper products (Gustafsson & Niskanen, 2012)

There has been a considerable increase in the use of paper in packaging, other branches such as food, hygiene products, and e-commerce, but a decline in the use of graphic papers (Barg & Oskar, 2019). There is a need to understand the use of paper in design better so that products made from it can have a long life and less impact on the environment. This can be only done by having good models for the constitutive behavior of paper that can be used to predict the behavior of the final product.

The final mechanical properties of paper are influenced by many parameters which can be environmental variables or process variables during papermaking. Some of the process variables in papermaking which can influence the properties of the paper include

- Pulp making process
- Beating of pulp
- Forming of fiber network
- Drying technique in papermaking
- Moisture content retention at the end of the papermaking

The environmental variables to which paper is sensitive are moisture and temperature. Among them, the moisture is more dominant, since the fibers interact with water molecules, and the network strength decreases. (Motamedian & Kulachenko, 2019)

1.2 MICROSTRUCTURE OF PAPERBOARD

The microstructure is the key to understand the mechanical response of any material. An important role is played by the nanostructure in some materials. A good example of that is nanomaterials.

The regular composite material treatment cannot be used for the paper. This is because of its peculiar microstructure and sometimes the nanostructure.

The properties of any network structure are defined by mainly

- Properties of a single fiber – defined by the nanofibrils
- The bond strength between the fibers in the network

The bond strength is affected by among others interacting water molecules, but also mechanical entanglement and other chemical bonds can play a role (Gustafsson & Niskanen, 2012).

1.3 INFLUENCE OF MOISTURE IN THE PAPER-MAKING PROCESS AND PACKAGING

Generally, the paper is highly hygroscopic in nature. This makes the paper susceptible to water molecules. Either the water molecules are saturated in the fiber walls or they can be free in the domain. The paper encounters moisture in almost all its lifetime. Two divisions can be made in the lifetime of paper. The first division is when the paper is made from the pulp. The drying and pressing technique allows the paper to have contact with water molecules. The other being the lifecycle of a finished paper product. The finished product is affected by the environmental conditions that include the moisture level.

The intake of moisture during pressing and drying techniques in the papermaking process generates three deformation patterns in the paper, which affect the process quality of the paper. They are curl, fluting, cockling which differ in length scale, and magnitude of deformation. (Kulachenko, 2012)

Once the paper is made, it could be converted to a packaging product. Since the paper is highly hygroscopic, the ambient moisture has a significant effect on the final properties of the packaging product. Uptake of water can affect both the fiber properties and the bond between fibers, which ultimately weakens the network strength and reduces the package performance.

1.4 SCOPE OF PROJECT

An experimental procedure at different controlled humidity environments shows that some of the mechanical in-plane properties of paperboard are a linear function of moisture ratio (Marin, Nygårds, & Östlund, 2020). The moisture ratio (m_r) of the paper and is defined as

$$m_r = \frac{m_w}{m_d} \tag{1.1}$$

where m_w is the mass of water and m_d is the mass of the dry solid content. The mass of water is calculated from the total mass, m_{total} , as

$$m_w = m_{total} - m_d \tag{1.2}$$

The relations are explained in detail in Section 2.2.

This master thesis project focusses on including this moisture scaling in both the elastic and plastic stress-strain response of paperboard. This is done by proposing a new and simplified flow rule which can account for these scaling factors and the model is verified against the experimental values.

In short, this thesis project can be summarized as

- Include moisture scaling in anisotropic elasticity
- Propose a new flow rule with moisture scaling for analysis of plasticity
- Verify this model on uniaxial samples in both MD and CD
- Verify this model on biaxially loaded samples.

The moisture also affects the creep behavior of the paper. The creep behavior of paper is observed to change drastically due to altering moisture levels. This acceleration of creep behavior is termed as mechanosorptive creep. Although moisture changes are not considered in the proposed model, this project can be seen as an initial step towards prediction of mechanosorptive creep.

2 LITERATURE REVIEW AND EXPERIMENTAL WORK

2.1 LITERATURE REVIEW

As paper cannot be considered as a metal or a fiber-reinforced polymer composite, there are different techniques available to model its mechanical behavior. Continuum Mechanics that are being applied to all kinds of solid materials have been extensively employed to model the anisotropic behavior of paper.

The most important one among those is perhaps the Xia – Nygårds model (Xia, Boyce, & Parks, 2002) (Nygårds, 2005) which has been used extensively to model the response of paperboard. In this model, the in-plane and out-of-plane responses are uncoupled and modeled using two sets of constitutive equations. The out of plane delamination behavior is modeled by an interface constitutive model. The in-plane elastic-plastic response is modeled by a 3D anisotropic continuum constitutive model, where the evolution of the yield surface is modeled by anisotropic hyperbolic strain hardening.

A simple anisotropic elastic model with a Hill yield surface has been used to model paperboard (Huang & Nygårds, 2010). An isotropic hardening is considered for the evolution of the yield surface. The softening effect observed in non-proportional loading of pre-strained samples is modeled using distortional hardening (Borgqvist, Lindström, Tryding, Wallin, & Ristinmaa, 2014). This model is an extension of the Xia – Nygårds model. The mechanical response of high-density cellulose-based materials considering rate-dependent formulation is proposed done by (Tjahjanto, Girlanda, & Östlund, 2015) using an approach based on the Xia – Nygårds model. To capture the hysteresis of the cellulose materials, kinematic hardening has also been modeled. The quadratic hardening model (Wallmeier, Linvill, Hauptmann, Majschak, & Östlund, 2015), (Linvill, Wallmeier, & Östlund, 2017) is extensively used in the analysis of deep drawing of paperboard.

Some of the other material models proposed in the literature include modeling paper as a network of fibers, nonlinear hardening for papers at different dry solid contents (Erkkilä, Leppänen, & Hämäläinen, 2013), Hill model with anisotropic hardening (Liu, Huang, & Stout, 1997), anisotropic plasticity at large strains (Harrysson & Ristinmaa, 2007), non-associative plasticity for the paper under in-plane loading (Pfeiffer & Kolling, 2019) and, transversely isotropic material with anisotropic hardening (Li, Guo, & Shim, 2018).

The advantage of using these models is that the elastic-plastic behavior of paper can be captured using only orthotropic elasticity and a flow rule. The major drawback of these kind of models is that they do not include the inhomogeneous nature of the paper or the microstructure of the paper.

Multi-scale modeling of paper is also gaining interest recently. Multiscale modeling of paper can be done by representing a random network of fibers and defining how the contact points between fibers behave (Borodulina, Kulachenko, Galland, & Nygårds, 2012), (Motamedian & Kulachenko, 2019). This kind of modeling is called fiber network modeling since it involves

going down one scale and fibers are modeled explicitly. This can help in tackling some of the problems that continuum mechanics is not able to do, such as include strength between individual fibers, and the random fiber network structure. The inhomogeneity problem can be solved by modeling a network of fibers. The main difficulty of this approach is to evaluate single fiber properties and the fiber-fiber joint strength distribution.

Molecular dynamics in paper research is also gaining some attraction. Molecular dynamics is essentially solving Newton's second law for many molecules as opposed to applying the same for a point in continuum mechanics. This can help to understand some questions that classical solid mechanics cannot answer. A single fiber consists of many molecules that in turn, can make the model complex and huge, which is a major limitation of this kind of modeling. (Khodayari, 2020)

Thus, finally, it is one's choice how to model the constitutive behavior of paper, and how much detailing is needed to understand the physics in relation to the particular application of interest.

2.2 EXPERIMENTAL BACKGROUND

An experimental study on paperboard at controlled humidity levels in both MD and CD samples is conducted by Marin et al. (2020). Different commercial paperboards from different producers and board machines are used. The selected paperboards have different types of fibers and different ply structures. They were chosen such that a large span in both mechanical properties and moisture dependency is observed. In addition, different grammages have been considered for each type of paperboard ranging from 180 to 350 g/m^2.

A bilinear elastic-plastic material is considered based on the mechanical properties: strength(σ_f), stiffness(E), yield strength (σ_y) and hardening modulus(H). The moisture ratio (defined in Section 1.4) is normalized with respect to moisture ratio at standard climate (50 % RH, 23 °C). The tests were performed at a different relative humidity (20, 50, 70, and 90 % RH) but with constant temperature (23 °C) in MD and CD, respectively. The mechanical properties were normalized with respect to the property at standard climate (50 % RH, 23 °C). It was observed that a linear response was able to fit the normalized mechanical property to the normalized moisture ratio according to

$$\frac{Property}{Property_{50\ RH}} = a_{property}\, m_r^n + b_{property}\ ;\ m_r^n = \frac{m_r}{m_{r\ 50\ RH}} \qquad (2.1)$$

where m_r is the moisture ratio at the required humidity level and $m_{r\ 50\ RH}$ is the moisture ratio at 50 % RH level and m_r^n is the normalized moisture ratio at the required humidity level.

The linear constants are presented with the coefficient of determination (R^2) in Table 2.1

Table 2.1 Relation between normalized mechanical property and normalized moisture ratio

	Mechanical Property	a_i	b_i	R_i^2
1	Strength (σ_f)	-0.35	1.36	0.96
2	Stiffness (E)	-0.37	1.40	0.96
3	Yield Stress (σ_y)	-0.50	1.55	0.93
4	Hardening modulus (H)	-0.43	1.49	0.88

The linear equation gives a good estimation of strength and stiffness. The yield stress and hardening modulus are seen to have low R^2. This makes the plastic response of paper, less accurate than the elastic response. The normalized stiffness as a function of normalized moisture ratio is shown in Figure 2.1.

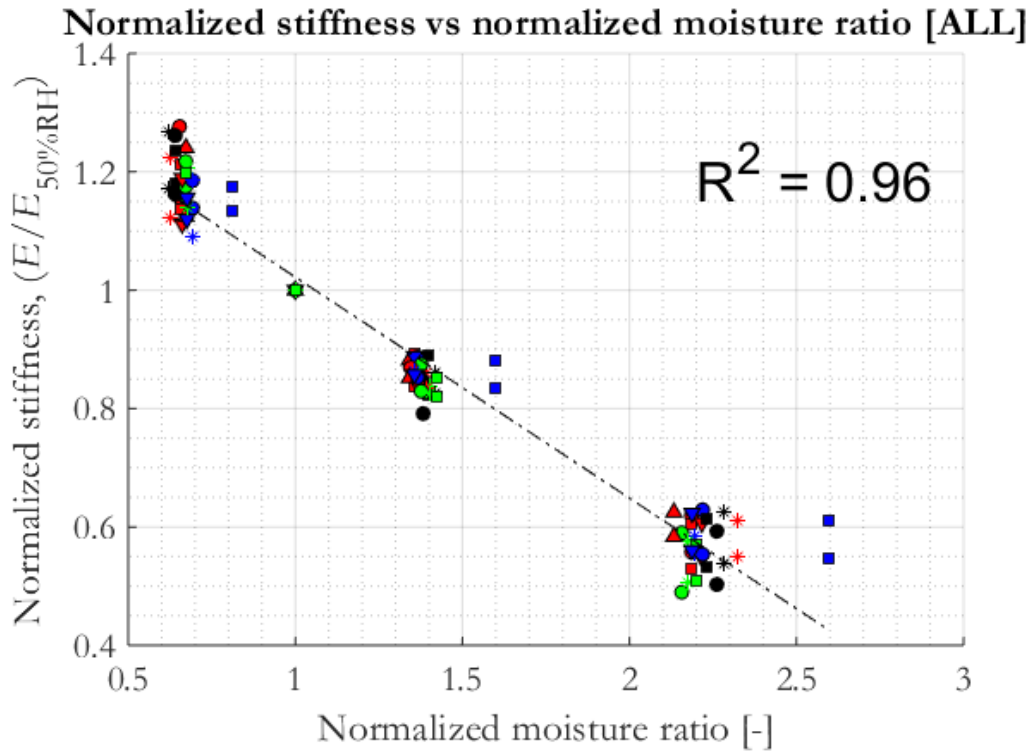

Figure 2.1 Normalized stiffness as a function of normalized moisture ratio for all boards in both MD and CD (Marin, Nygårds, & Östlund, 2020)

From the experimental background and literature review, it is evident that a new model is needed to simulate the effect of moisture. The new model should be simple to implement in any commercial finite element software and need to consider the moisture scaling of the constitutive parameters.

3 METHOD

From the experimental work, it is clear that the moisture dependent in plane model should include

- Orthotropic elasticity where all elastic constants are functions of moisture ratio
- Anisotropic linear hardening plasticity with the hardening modulus being a function of moisture ratio

3.1 THEORY OF PROPOSED MODEL

The topic of interest is to model the in-plane response of paper, out-of-plane properties are not considered. The in-plane response can be calculated using plane stress approach, but a full orthotropic model is taken into consideration in this project. This is done to accommodate future work where out of plane response can be included.

The response curve for a sample in the MD is shown in Figure 3.1.

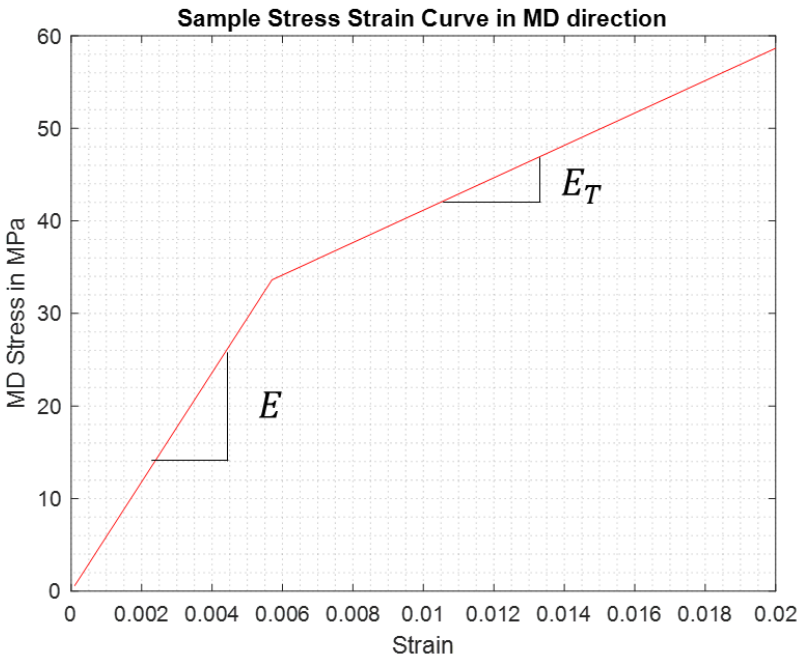

Figure 3.1 Bi-linear elastic plastic model

The first linear slope corresponds to the elastic modulus, E, and the second linear slope corresponds to the tangent modulus, E_T. The tangent modulus, E_T, in this case can be computed as

$$\frac{1}{E_T} = \frac{1}{E} + \frac{1}{H} \tag{3.1}$$

where H is the hardening modulus (see Section 3.1.2.1)

3.1.1 ORTHOTROPIC ELASTICITY

In general, the elastic representation of paperboard is represented by an orthotropic behavior. The relation between stress and strain components for an orthotropic elastic material in Voigt notation can be written as

$$\{\epsilon\} = [L][C]^{-1}[L]^T\{\sigma\} \tag{3.2}$$

where $\{\epsilon\}$ is the engineering strain vector in Voigt notation, $[L]$ is the transformation matrix required to transform into the global material direction, $[C]^{-1}$ is the inverse of stiffness matrix or compliance matrix in the local coordinate system and $\{\sigma\}$ is the stress tensor written in Voigt notation.

For an orthotropic material, the compliance matrix is given by

$$[S] = [C]^{-1} = \begin{bmatrix} \frac{1}{E_x} & \frac{-v_{xy}}{E_x} & \frac{-v_{xz}}{E_x} & 0 & 0 & 0 \\ \frac{-v_{yx}}{E_y} & \frac{1}{E_y} & \frac{-v_{yz}}{E_y} & 0 & 0 & 0 \\ \frac{-v_{zx}}{E_z} & \frac{-v_{zy}}{E_z} & \frac{1}{E_z} & 0 & 0 & 0 \\ 0 & 0 & 0 & \frac{1}{G_{xz}} & 0 & 0 \\ 0 & 0 & 0 & 0 & \frac{1}{G_{yz}} & 0 \\ 0 & 0 & 0 & 0 & 0 & \frac{1}{G_{xy}} \end{bmatrix} \tag{3.3}$$

Here x represents the MD, y represents the CD and z represents ZD as illustrated in Figure 1.1. Nine material parameters are required for a complete representation of an orthotropic material.

From the experimental work mentioned in Section 2.2, the elastic modulus can be written as

$$E_i = (a_2 m_r^n + b_2) E_i^{50\%} \tag{3.4}$$

where $E_i^{50\%}$ is the elastic modulus determined from experiments at 50% RH, a_2 , b_2 are the constants determined in the fitting curve for the stiffness (Table 2.1) and m_r^n is the normalized moisture ratio at the required humidity level.

Determination of Elastic Constants:

The elastic constants to be determined for an orthotropic elasticity are $E_x, E_y, E_z, v_{xy}, v_{yz}, v_{zx}, G_{xy}, G_{yz}, G_{zx}$.

The in-plane elastic moduli (E_x, E_y) can be estimated from the experimental data of uniaxial tensile tests (see Section 4.1).

The other in plane constants (v_{xy}, G_{xy}) can be estimated from (Baum, Brennan D, & Habeger, 1981)

$$v_{xy} = 0.293\sqrt{\frac{E_x}{E_y}}$$
$$G_{xy} = 0.65\sqrt{E_x E_y} \quad (3.5)$$

Since the objective of this project is focused on assessing the in–plane response, the out of plane properties are assigned values that should not influence the in-plane solution. However, if there is a need for estimating the out–of plane properties the reader is referred to Nygårds (2008) for more information.

3.1.2 ANISOTROPIC HARDENING

A simple yield criterion that accounts for the orthotropy in paper materials is assumed. To include the hardening modulus in all directions, the flow rule can be assumed as

$$f = \frac{\sigma_i^2}{\left(\sigma_i^s(m_r)\right)^2} = \left(\frac{\sigma_x}{\sigma_x^s}\right)^2 + \left(\frac{\sigma_y}{\sigma_y^s}\right)^2 + \left(\frac{\sigma_z}{\sigma_z^s}\right)^2 + \left(\frac{\sigma_{xy}}{\sigma_{xy}^s}\right)^2 + \left(\frac{\sigma_{xz}}{\sigma_{xz}^s}\right)^2 + \left(\frac{\sigma_{yz}}{\sigma_{yz}^s}\right)^2 = 1 \quad (3.6)$$

where $\sigma_x, \sigma_y, \sigma_z, \sigma_{xy}, \sigma_{xz}, \sigma_{yz}$ are the components of the stress tensor. The flow stress is assumed to be given by

$$\sigma_i^s(m_r) = \sigma_i^y(m_r) + H_i(m_r)\epsilon_i^p \quad (3.7)$$

where $\sigma_i^y(m_r)$ corresponds to the yield stress, $H_i(m_r)$ is the hardening modulus and ϵ_i^p is the accumulated plastic strain in *'i'* direction. It should be noted that both the yield stress and hardening modulus are functions of moisture ratio.

Assuming an associative flow rule[3], the plastic strain increment can be written as

$$d\epsilon_i^p = d\lambda \frac{\partial f}{\partial \sigma_i} \quad (3.8)$$

where $d\lambda$ is the plastic multiplier, and $\frac{\partial f}{\partial \sigma_i}$ is the gradient of flow rule with the respective stress.

[3] Associative flow rule – Plastic evolution normal to flow (or yield) surface

3.1.2.1 Definition of hardening modulus:

For an isotropic hardening behavior, the hardening modulus is defined as

$$H = \frac{d\sigma_{eff}}{d\epsilon^p_{eff}} \tag{3.9}$$

For an anisotropic hardening behavior, there are different hardening moduli in the different directions. In analogy with isotropic hardening, the hardening modulus for an anisotropic material is defined in all material directions as

$$H_i = \frac{d\sigma_i}{d\epsilon^p_i} \tag{3.10}$$

As a simplification, the model only two considers two hardening moduli and the remaining four are assumed zero. The two hardening moduli considered are for the directions x and y (which are essentially MD and CD for paperboard).

$$H_x = \frac{d\sigma^p_x}{d\epsilon_x}\,; H_y = \frac{d\sigma^p_y}{d\epsilon_y} \qquad H_{xy} = H_{yz} = H_{zx} = H_z = 0 \tag{3.11}$$

3.2 IMPLEMENTATION

Since the topic of interest is in the mechanical response of paper (stress state, elastic strain, and plastic strain) when loads and displacements are applied, the problem to solve becomes a boundary value problem.

The constitutive equations defined in Section 3.1.1 and 3.1.2 and the general structural geometries to be considered are far too complicated to solve with an exact analytical approach. Therefore, an approximate numerical method is needed. The most widely used in solving boundary value problems in solid mechanics is the finite element (FE) method.

The FE method is a numerical tool that is used to solve differential equations over a domain. In the FE method, the domain is discretized into small domains called finite elements. The finite elements can be a line element (1D), a planar element (2D) or a solid element (3D). This has to be properly selected based on the problem. The variables to solve for (typically displacements in solid mechanics problems) are then approximated with (e.g. linear, quadratic, etc.) interpolations over the elements. The interpolation functions need to be properly defined such that they can capture the variation of the variable in that particular element. The interpolation of the required variable makes the problem simpler because the continuous variable is approximated with simple polynomials. By assembling the stiffness properties and loads on all elements, a system of linear or non-linear equations is obtain. In general, many methods can be used to solve these systems of equations using computers.

The system of equations needed for the finite element method to be solved in solid mechanics problems is generally generated using the principle of virtual work or calculus of variations. More information about FEM can be found in Zienkiewicz. et al. (2013) and Bonet & Wood (1997).

3.2.1 STRESS INTEGRATION

The basic principle of FEM can be simply put in terms of the work done by the external forces equals the work done by internal forces

$$P_I = P_E \tag{3.12}$$

where P_I is the internal work done and P_E is the external work done.

$$P_I = \int_{\Omega} [B]^T [\sigma] \; dv$$

$$P_E = \int_{\delta\Omega_t} [N]^T t \; ds + \int_{\Omega} [N]^T b_f \; dv \tag{3.13}$$

where $[N]$ is the displacement interpolation matrix, $[B]$ is the strain -displacement matrix and $[\sigma]$ is the stress-state written in Voigt notation. The traction vector is denoted by t and b_f is the body force vector.

For the non – linear case, generally, an incremental procedure is used, which means that the load is applied in increments, and an iterative procedure is solved for fulfilling the equilibrium.

The equation to solve becomes

$$\dot{P}_I = \dot{P}_E \Rightarrow \int_{\Omega} [B]^T \dot{\sigma} \, dv = \dot{P}_E$$

Nonlinear problems in solid mechanics can be classified into three types.

- Geometric nonlinearity – large deformations
- Material nonlinearity – the material behaves nonlinearly
- Contact nonlinearity – two bodies in contact

Any combination of above-mentioned three nonlinear varieties can be present in a problem. In this project, only material non-linearity is accounted for.

The finite element equations can be solved using either an implicit or an explicit formulation. These resemble the backward and forward Euler methods known from applied mathematics. An implicit type of problem-solving starts with a value being assumed and iterated until global equilibrium is established. In the explicit type of problem solving, the solution for the next step is predicted directly from the already known values. Both have their advantages and

disadvantages. More on that can be found in Bonet & Wood (1997) and Zienkiewicz, Taylor, & Zhu (2013). In this project, the problem is solved using the implicit method and the solution procedure for that is discussed here, only. All equations derived are based on the information provided in Gudmundson (2010).

A complete nonlinear implicit finite element problem is composed of two steps

- The solution of the global equilibrium for each load increment
- Integration of the constitutive equations at every material point (i.e. every Gauss point).

The integration of the constitutive equations is not present in a linear problem because the material has not yet yielded. Thus, the displacements, strains and stresses follow directly from the solution of the linear system of equations.

The global equilibrium for the next step is attained and can be written at time step *'n'* as

$$\Delta P_I = \Delta P_E \tag{3.14}$$

For the next time step, generally an iterative procedure is used. The value to be solved is the displacement increment for the next time step. This is assumed zero at the start of the iteration.

For time step *'n+1'* at the i^{th} iteration

$$\left|\Delta P_I|_{n+1}^{i} - \Delta P_E|_{n+1}^{i}\right| = \Delta R|_n^i \tag{3.15}$$

where $\Delta R|_n^i$ is the residual between change in internal and external work done at i^{th} iteration. Ideally, it is required and essential that $\Delta R|_{n+1}^{i} = 0$, but a tolerance *'tol'* is generally kept

$$\left|\Delta R|_{n+1}^{i}\right| < tol \tag{3.16}$$

The next iteration in this time step can be written as

$$\begin{gathered}\Delta D|_n^{i+1} = \Delta D|_n^i - \frac{\Delta R_n\left(\Delta D|_n^i\right)}{\left(\frac{\mathrm{d}\Delta R_n}{d\Delta D|_n^i}\right)} \\ \Rightarrow\ \Delta D|_n^{i+1} = \Delta D|_n^i - \left[K_{NR}^i\right]_n^{-1}\Delta R_n\left(\Delta D|_n^i\right)\end{gathered} \tag{3.17}$$

where $\Delta D|_n^{i+1}$is the solution for next iteration, $\Delta D|_n^i$ is the solution for the previous iteration and $\left[K_{NR}^i\right]_n$ is called the algorithmic tangent stiffness.

The algorithmic tangent stiffness can be expressed as

$$\left[K_{NR}^i\right]_n = \frac{d\Delta R_n}{d\Delta D|_n^i} = \int_{\Omega} [B]^T \frac{d\Delta\sigma_n^i}{d\Delta D_n^i}\, dv \tag{3.18}$$

Efficient calculation of this matric requires evaluation of stress at *'n+1'* time step accurately. This can be done by either implicit or explicit type of stress integration.

Implicit integration of stress is used in this project. One commonly used method for implicit integration of stress is known as radial return mapping in computational inelasticity terms and it can be simply put in words as

- Assume a trial stress state assuming elasticity
- Check the flow rule and bring back the updated stress on to the yield (or flow) surface
- Update the values and continue the loop until a certain tolerance is achieved

The linear elastic trial stress state is defined as

$$\bar{\sigma}_{n+1}^{i} = [\boldsymbol{C}(m_r)]\bar{\varepsilon}^{i}_{n+1} = [\boldsymbol{C}(m_r)][\boldsymbol{B}]\, D^{i}_{n+1}\,;\; D^{i}_{n+1} = D_n + \Delta D^{i}_{n} \tag{3.19}$$

where D_n is the converged displacement from the n^{th} time step, ΔD_n^i is the i^{th} iteration of displacement increment for the next time step.

Then the flow rule corresponding to the material model is checked with the trial stress state as

$$f^{i}_{n+1} = \sum_{i=1}^{6} \frac{\left(\bar{\sigma}^{i}_{n+1}\right)^2}{\left(\sigma_i^{s,n}(m_r)\right)^2} - 1 \tag{3.20}$$

where $\sigma_i^{s,n}(m_r)$ is the flow stress at the n^{th} time step. The flow stress is calculated from Equation (3.7). The plastic strains are added iteratively after each converged solution.

1. If $\left(f^{i}_{n+1} < 0\right)$, then the iterative stress integration is not required, and the trial stress state is the final solution for that time step.
2. Else, the stress state has to be brought back on the yield surface. This is done as

$$\epsilon^{tot} = \epsilon^{el} + \epsilon^{p} + \epsilon^{mr} \tag{3.21}$$

where ϵ^{tot} is the total strain, ϵ^{el} is the elastic component, ϵ^{p} is the plastic component and ϵ^{mr} is the swelling component due to moisture change.

Moisture change is not considered in this project since the experiments were performed at stationary moisture conditions. Thus, the total strain can be written as

$$\epsilon^{tot} = \epsilon^{el} + \epsilon^{p} \tag{3.22}$$

Multiplying with the stiffness matrix on both sides yields

$$\begin{gathered} [\boldsymbol{C}(m_r)]\epsilon^{tot} = [\boldsymbol{C}(m_r)]\epsilon^{el} + [\boldsymbol{C}(m_r)]\epsilon^{p} \\ \Rightarrow\; \bar{\sigma}^{i}_{n+1} = \sigma^{i}_{n+1} - \;[\boldsymbol{C}(m_r)]\epsilon^{p} \end{gathered} \tag{3.23}$$

where σ^{i}_{n+1} is the stress for the i^{th} the iteration at time step $n+1$.

In the implicit integration, the accumulated plastic strain can be written as

$$\sigma_{n+1}^{i} = \bar{\sigma}_{n+1}^{i} - [\boldsymbol{C}(m_r)] \int_{\bar{\varepsilon}_n^p}^{\bar{\varepsilon}_{n+1}^p} \dot{\varepsilon}^p \, dt \tag{3.24}$$

From the definition of the updated flow rule

$$f = \sum_{i=1}^{6} \frac{\sigma_i^2}{\left(\sigma_i^{s,n}(m_r) + H_i(m_r)\Delta\epsilon_i^{p,n}\right)^2} - 1 = 0 \tag{3.25}$$

where $\sigma_i^{s,n}(m_r)$ is the flow stress at the n^{th} time step and $\Delta\epsilon_i^{p,n}$ is the increment of plastic strain during this time step.

Following an associative flow rule, the plastic gradient can be written as

$$\dot{\varepsilon}^p = \dot{\lambda} \left.\frac{\partial f}{\partial \sigma}\right|_n^i$$

$$\left.\frac{\partial f}{\partial \sigma}\right|_n^i = \frac{2\sigma_i}{\left(\sigma_i^{s,n} + H_i\Delta\epsilon_i^{p,n}\right)^2} - \frac{2\sigma_i^2\left(H_i \dfrac{d\Delta\epsilon_i^{p,n}}{d\sigma_i}\right)}{\left(\sigma_i^{s,n} + H_i\Delta\epsilon_i^{p,n}\right)^3} \tag{3.26}$$

This can be simplified as (See Section A.1 for complete derivation)

$$\dot{\varepsilon}_i^p = d\lambda \left[\frac{2\sigma_i}{\left(\sigma_i^{s,n} + H_i\Delta\epsilon_i^{p,n}\right)^2} - \frac{2\sigma_i^2}{\left(\sigma_i^{s,n} + H_i\Delta\epsilon_i^{p,n}\right)^3}\right] \tag{3.27}$$

Assuming that the gradient is constant during the step which means that only small steps can be taken in simulation, Equation (3.24) can be approximated in Voight notation as

$$\sigma_i = \bar{\sigma}_i - \boldsymbol{C}_{ij}(m_r)\left[\frac{2\sigma_j}{\left(\sigma_j^{s,n} + H_j\Delta\epsilon_j^{p,n}\right)^2} - \frac{2\sigma_j^2}{\left(\sigma_j^{s,n} + H_j\Delta\epsilon_j^{p,n}\right)^3}\right] \tag{3.28}$$

The incremental plastic strain $\Delta\epsilon_j^{p,n}$ is an unknown to be solved for from the stress state. This term being in denominator makes solving for $\Delta\epsilon_j^{p,n}$ even more complicated. Small steps are already taken into consideration to simplify the Equation (3.24) to (3.28) and this is further motivated by this assumption.

$$\sigma_j^{s,n} + H_j\Delta\epsilon_j^{p,n} \cong \sigma_j^{s,n} \tag{3.29}$$

Finally, with all assumptions from Equations (3.26) to (3.29), the main Equation (3.24) can be rewritten as

$$\left[(\delta_{ij})\sigma_j + \left[\frac{2\,\boldsymbol{C}_{ij}\,\sigma_j}{\left(\sigma_j^{s,n}\right)^2} - \frac{2\,\boldsymbol{C}_{ij}\,\sigma_j^2}{\left(\sigma_j^{s,n}\right)^3}\right]\Delta\lambda_n\right] = \bar{\sigma}_{ij} \tag{3.30}$$

In matrix notation, this can be written as

$$(I + 2D\Delta\lambda_n)\,\sigma - 2E\Sigma(\sigma^2)\Delta\lambda_n = \bar{\sigma} \parallel D_{ij} = \frac{\boldsymbol{C}_{ij}}{\left(\sigma_j^{s,n}\right)^2}\,; E_{ijkl} = \frac{\boldsymbol{C}_{ij}}{\left(\sigma_j^{s,n}\right)^3} \tag{3.31}$$

where $\Sigma(\sigma^2)$ is another stress tensor where every element in the original stress tensor is squared.

$$\Sigma_i = \sigma_i^2 \tag{3.32}$$

Equations (3.25) and (3.30) constitutes a system of equations for the variables $x\ (7 \times 1)$

$$x = \begin{bmatrix} \sigma_{kl} \\ \Delta\lambda_n \end{bmatrix}$$

The complete system of equations in the Voigt notation be written as

$$F = \begin{bmatrix} \left[\delta_{ij} + 2D_{ij}\Delta\lambda_n\right]\sigma_j - 2E_{ij}\sigma_j^2\Delta\lambda_n - \bar{\sigma}_i \\ \sum_{i=1}^{6}\left[\dfrac{\sigma_i}{\sigma_i^{s,n} + H_i\,\Delta\epsilon_i^P(\Delta\lambda_n)}\right]^2 - 1 \end{bmatrix} = 0 \;\Bigg\|\; x = \begin{bmatrix} \sigma_i \\ \Delta\lambda_n \end{bmatrix} \tag{3.33}$$

This system of equations can be solved using many techniques for root finding. The most primitive one can be trial and error which is cumbersome and not advised because the same equation has to be solved for many elements in the FE problem. The most commonly used technique to solve this is the Newton-Raphson method which earlier was used in finding the displacement increment. This constitutes an internal Newton-Raphson method which is employed at Gauss point level, whereas the earlier one is at the global level employed after assembling the stiffness matrix of the complete system.

The next iteration for the state variables can be computed as

$$x_{s+1} = x_s - \left(\frac{dF}{dx}\right)_s^{-1} F_s \tag{3.34}$$

The evaluation of gradient $\frac{dF}{dx}$ is essential to compute the next iteration. This matrix can be computed every time for the iteration or can be computed at the start of the iteration. The one-time computation method is called Modified Newton Raphson Method. This usually takes more iterations than the general Newton-Raphson Method. The gradients evaluated for the general Newton- Raphson Method are presented in A.2.

3.2.2 ALGORITHM TANGENT STIFFNESS

After a successful evaluation of stress state and incremental plastic strain for the next iteration, the immediate step would be to formulate the algorithmic tangent stiffness presented in Equation (3.18). After some manipulations, the algorithmic tangent stiffness can be rewritten as

$$\left[K_{NR}^{i}\right]_{n} = \frac{d\Delta R_n}{d\Delta D|_n^i} = \int_{\Omega} [B]^T \frac{d\Delta\sigma_n^i}{d\Delta D_n^i}\, dv = \int_{\Omega} [B]^T \frac{\partial\Delta\sigma_n^i}{\partial\Delta\varepsilon_n^i}\frac{d\Delta\varepsilon_n^i}{d\Delta D_n^i}\, dv$$

$$\left[K_{NR}^{i}\right]_{n} = \int_{\Omega} [B]^T \frac{\partial\Delta\sigma_n^i}{\partial\Delta\varepsilon_n^i}\,[B]\, dv \tag{3.35}$$

The only unknown in this evaluation is the gradient of change in stress to change in strain which is called the Jacobian matrix.

To evaluate this Jacobian matrix, all equations used in a computing stress state and incremental plastic strain has to be written in differential form. The equations used are

$$\left[\delta_{ij} + 2D_{ij}\Delta\lambda_n\right]\sigma_j - 2E_{ij}\sigma_j^2\Delta\lambda_n = \bar{\sigma}_i\,;\ \bar{\sigma}_i = C_{ij}\varepsilon_j \tag{3.36}$$

$$f\left(\sigma_i\,, \Delta\lambda_n, \sigma_i^s(m_r), H_i(m_r)\right) = \sum_{i=1}^{6}\left[\frac{\sigma_i}{\sigma_i^{s,n} + H_i\,\Delta\epsilon_i^p}\right]^2 - 1 = 0 \tag{3.37}$$

Using Equations (3.36) and (3.37) in differential form and also consistency condition, it can be written as (See Section A.3 for more details)

$$\left(\delta_{ij} + \left[2D_{ij} + 4E_{ij}\sigma_j\right]\Delta\lambda_n\right)d\sigma_j = C_{ij}d\epsilon_j + \left[2D_{ij}\sigma_j + 2E_{ij}\sigma_j^2\right]\frac{(\nabla f_{n+1}^T)^i d\sigma}{\left(\frac{\partial f}{\partial(\Delta\lambda_n)}\right)} \tag{3.38}$$

where $(\nabla f_{n+1}^T)^i = \left[\frac{\partial f}{\partial\sigma_1} \quad \cdots \quad \frac{\partial f}{\partial\sigma_6}\right]$ is the gradient of flow rule with respect to the stress state and $\frac{\partial f}{\partial(\Delta\lambda_n)}$ is the gradient of flow rule with respect to the incremental effective plastic strain

This equation is made simpler by introducing the two matrices

$$\begin{aligned} G_{ij} &= \delta_{ij} + \left[2D_{ij} + 4E_{ij}\sigma_j\right]\Delta\lambda_n \\ L_{ij} &= \frac{1}{\left(\frac{\partial f}{\partial(\Delta\lambda_n)}\right)}\left[2D_{ij}\sigma_j + 2E_{ij}\sigma_j^2\right] \end{aligned} \tag{3.39}$$

Using Equation (3.39), the Equation (3.38) can be rewritten as

$$G_{ij}\, d\sigma_j = C_{ij}d\epsilon_j + L_{ij}(\nabla f_{n+1}^T)^i d\sigma_j \Rightarrow \left[G - L(\nabla f_{n+1}^T)^i\right]d\sigma = Cd\varepsilon$$

$$\Rightarrow d\sigma = \left[G - L(\nabla f_{n+1}^T)^i\right]^{-1}C\ \ d\varepsilon = \frac{\partial\Delta\sigma_n^i}{\partial\Delta\varepsilon_n^i}\, d\varepsilon$$

Finally, the Jacobian matrix can be written as

$$\frac{\partial\Delta\sigma_n^i}{\partial\Delta\varepsilon_n^i} = \left[G - L(\nabla f_{n+1}^T)^i\right]^{-1}C \tag{3.40}$$

The stress integration algorithm is summarized in Table 3.1

Table 3.1 Summary of Stress Integration method

1. Compute *trial elastic stress*

$$D_{n+1}^{i} = D_n + \Delta D_n^{i} \; ; \; \bar{\varepsilon}^{i}_{n+1} = [\boldsymbol{B}]\, D_{n+1}^{i}$$
$$\bar{\sigma}_{n+1}^{i} = [\boldsymbol{C}(m_r)]\bar{\varepsilon}^{i}_{n+1} = [\boldsymbol{C}(m_r)][\boldsymbol{B}]\, D_{n+1}^{i}$$

2. Update *flow stress* from previously converged solution

$$\sigma_i^{s,n}(m_r) = \sigma_i^{s,n-1}(m_r) + H_i(m_r)\Delta\epsilon_i^{p,n-1}$$

3. Check yield condition

$$f_{n+1}^{i} = \sum_{i=1}^{6} \frac{\left(\bar{\sigma}_{n+1}^{i}\right)^2}{\left(\sigma_i^{s,n}(m_r)\right)^2} - 1$$

IF $f_{n+1}^{i} \leq 0$ THEN:

$$\sigma_{n+1}^{i} = \bar{\sigma}_{n+1}^{i} \;\&\; \text{EXIT}$$

ENDIF

4. Compute the system of equations from r*adial return method*

$$F = \begin{bmatrix} \left[\delta_{ij} + 2D_{ij}\Delta\lambda_n\right]\sigma_j - 2E_{ij}\sigma_j^2\Delta\lambda_n - \bar{\sigma}_i \\ \sum_{i=1}^{6}\left[\dfrac{\sigma_i}{\sigma_i^{s,n} + H_i\,\Delta\epsilon_i^{P}(\Delta\lambda_n)}\right]^2 - 1 \end{bmatrix} = 0 \;\Bigg\|\; x = \begin{bmatrix} \sigma_i \\ \Delta\lambda_n \end{bmatrix}$$

5. Solve this system of equations iteratively using Newton Raphson method

$$x_{s+1} = x_s - \left(\frac{dF}{dx}\right)_s^{-1} F_s$$

6. Compute the *consistent tangent modulus* for this iteration for all Gauss points

$$\frac{\partial\Delta\sigma_n^{i}}{\partial\Delta\varepsilon_n^{i}} = \left[G - L(\nabla f_{n+1}^{T})^{i}\right]^{-1} C$$

$$G_{ij} = \delta_{ij} + \left[2D_{ij} + 4E_{ij}\sigma_j\right]\Delta\lambda_n \; ; L_{ij} = \frac{1}{\left(\dfrac{\partial f}{\partial(\Delta\lambda_n)}\right)}\left[2D_{ij}\sigma_j + 2E_{ij}\sigma_j^2\right]$$

The proposed model has not been checked for the principles of thermodynamics. Therefore, care must be taken when using this implemented model for problems with multiaxial loading and unloading.

3.3 IMPLEMENTATION IN LS-DYNA®

The equations derived in Section 3.2 needs to be implemented in a commercial Finite Element software. Some of the major software available for implementing user – defined material models are LS – DYNA®, ABAQUS®, ANSYS® and COMSOL®. All have their advantages and disadvantages. LS – DYNA® is chosen for this project to implement the material model. There might be a difference while implementing the same in any other software.

3.3.1 USER DEFINED FEATURES IN LS-DYNA®

There are many pre – defined models in LS – DYNA® which can be used to solve problems in different fields. There is also a provision for the user to define fully customized building blocks, like material models, elements, friction models and loadings see LS-DYNA Keyword User's Manual I (2019) and Erhart (2010) for more information. The user-defined models are plugged into LS – DYNA® via user subroutines written in FORTRAN 90. More information on the user-defined features can be found in Appendix A-H of LS-DYNA Keyword user's anual I (2019).

The user-defined subroutines are compiled using the object version of LS – DYNA® (see Figure 3.2) where the necessary coding must be done. Since the coding is completely done in FORTRAN, an external compiler is needed. The general ones include Intel FORTRAN Compiler (which is a part of Intel Parallel Studio), GNU compiler. For each variant of LS – DYNA® there is a particular set of Intel FORTRAN Compiler and Microsoft Visual C++ needed for linking and accessing the standard libraries. The recommended FORTRAN compiler for *LS-DYNA R11* is *Intel Parallel Studio XE 2017* and the corresponding Microsoft application environment is *Microsoft Visual C++ 2017 x64 Cross Tools*.

The procedure for writing the user-defined subroutines varies for the LINUX and Windows operating systems, respectively. In LINUX, a module can be defined that can help facilitate working with User Defined Functions (UDFs). The work involved with defining UDFs is significantly reduced such that the whole usermat package (see Figure 3.2) need not be used for generating executable file but can be concise and replaced by *MODULE keywords (see Figure 3.3).

The provision of the module concept is not available the Windows, so the normal procedure of changing the source codes and compiling them to get the executable file should be used. This is not as flexible as the '*module*' concept and if there are many UDFs in a model, it is advised to use the '*module*' concept in the LINUX environment. The material model in this project is implemented for Windows.

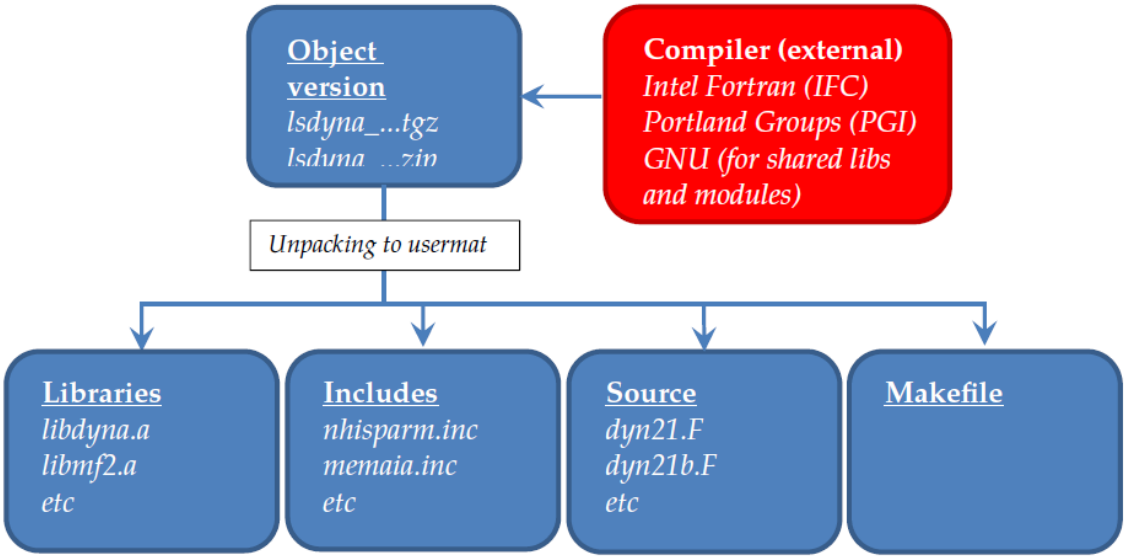

Figure 3.2 Details of Object Version in LS – DYNA® (LS-DYNA Keyword User's Manual I (2019))

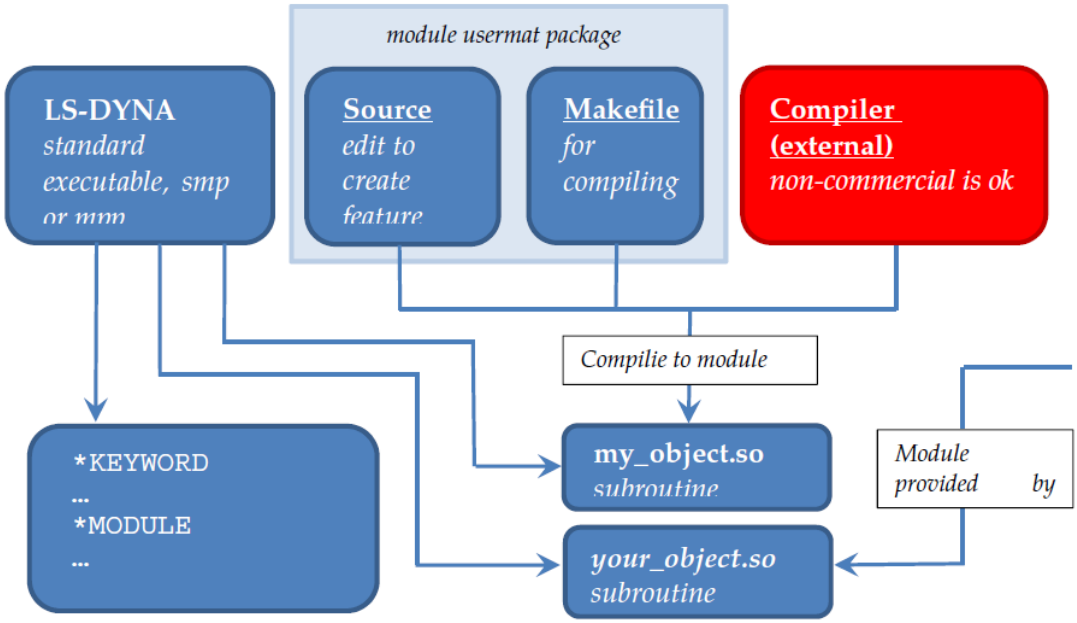

Figure 3.3 Module Concept used for LINUX environments (LS-DYNA Keyword User's Manual I (2019))

Implementing any UDF is complicated, and a stepwise fashion to increase the complexity level is adopted which can be easy to implement and better for debugging. For example, in the User Defined Material Model (UMAT), an elastic solution is implemented first and then the yield condition with perfect plasticity is implemented and finally the hardening behavior.

3.3.2 USER DEFINED MATERIAL MODELS IN LS – DYNA®

The major and the most common one of UDFs is the User Defined Material Model (UMAT). If the available material models are not sufficient to capture the material behavior, then a UMAT is to be implemented. The UMAT can be implemented for an explicit or an implicit cycle, respectively. For an explicit cycle, only a stress update (see Section 3.2.1) for the next time step is sufficient whereas for the implicit cycle including the stress update the consistent tangent matrix (see Section 3.2.2) also has to be updated.

The implicit sequence is defined in the user-defined material subroutine umat*XX* (where 41 ≤ *XX* ≤ 50), with the strain rate (or deformation gradient) as the main input. The main objective of this subroutine is to update the (Cauchy) stress and any history dependent variables required for the next time step. The input quantities in this subroutine are in the local element coordinate system. This is illustrated in Figure 3.4.

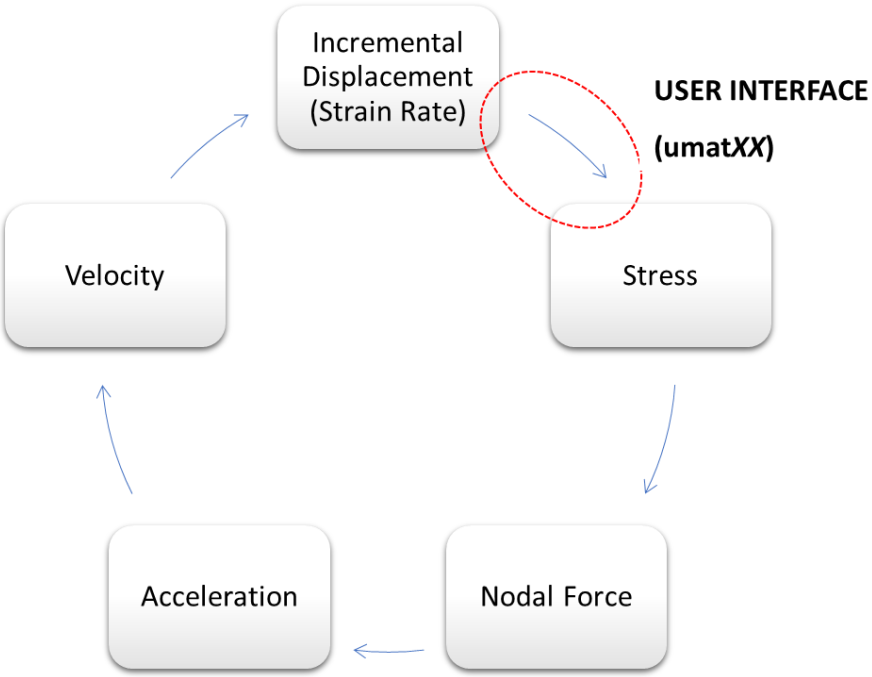

Figure 3.4 Finite Element Method for Explicit Method with User-Defined Material Model

When implementing the material model for shells and beams, the stresses that are consistent with the assumptions according to structural elements ($\sigma_{33} = 0$ for shells) is implemented in the corresponding umat*XX*.

For an implicit method, apart from the stress update the material stiffness matrix is to be implemented in the corresponding subroutine utan*XX*. This subroutine is called when assembling the global stiffness matrix. This is shown in Figure 3.5.

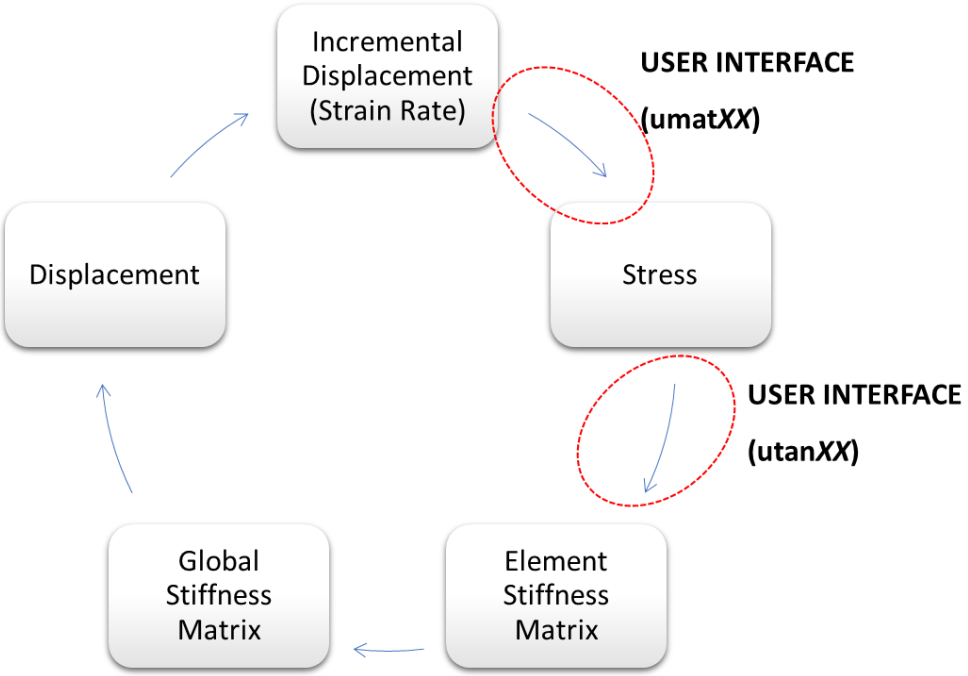

Figure 3.5 Finite Element Method for Implicit Method with User-Defined Material Model

In this project all of the simulations are done in implicit mode. Both user-defined features, UMAT and UTAN, are needed. The stress integration method with Newton – Raphson method in Section 3.2.1 is implemented in umat*XX*. The tangent stiffness derived in Section 3.2.2 is implemented in utan*XX*.

3.4 UNIAXIAL SPECIMEN

The implemented model is verified on the uniaxial specimen used for experiments. It is shown with dimensions in Figure 3.6.

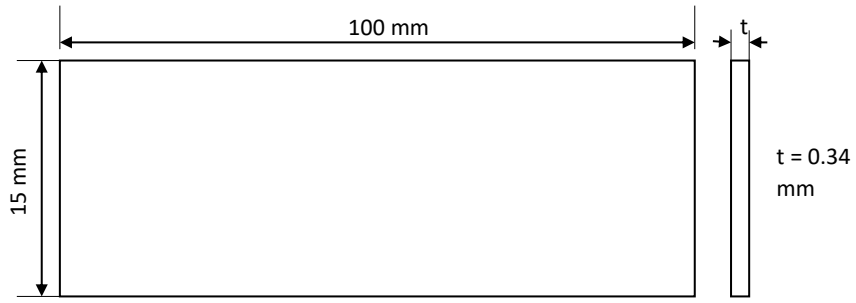

Figure 3.6 Uniaxial specimen used for both MD and CD testing

The uniaxial specimen can be modeled two ways i.e. modeling the complete specimen, fixing one end, and applying load at the other end. The full sample modeled with boundary conditions is shown in Figure 3.7.

The other approach is to model the only a quarter of the specimen and applying the symmetry boundary conditions. For MAT157 both approaches have very small differences in

computation time, but for UMAT the full specimen takes a lot more execution time[4] than the symmetry one. Therefore, the UMAT simulations are done with the quarter-symmetry model to reduce the execution time. The symmetry sample with boundary conditions is shown in Figure 3.8.

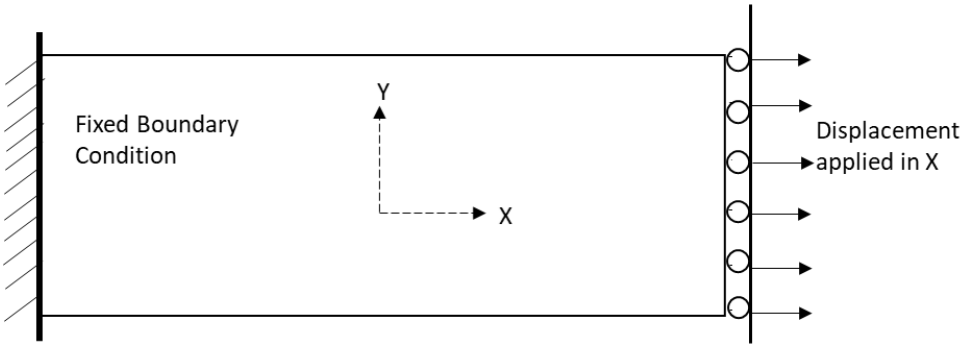

Figure 3.7 Full Sample modelled with boundary conditions

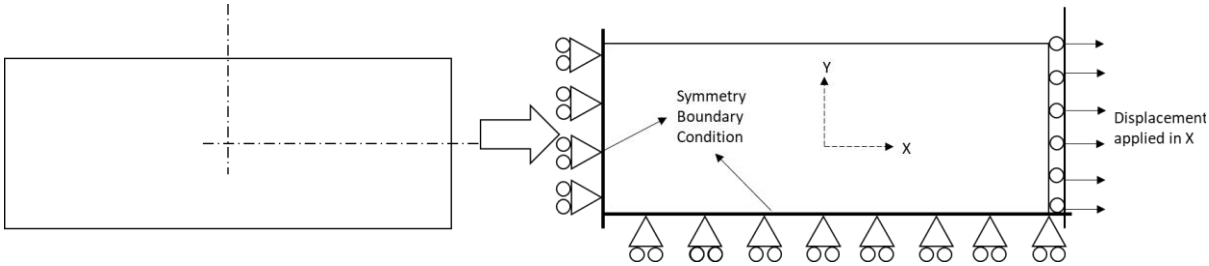

Figure 3.8 Symmetry sample with boundary conditions

Generally, shell elements have been used to model the paper for both MAT 157 and UMAT simulations. Due to some implementation problems, solid elements are used for UMAT (discussed more in Section 6). These simulations are done with a fully integrated shell (ELFORM[5] 2 in LS-DYNA®) and solid elements (ELFORM 16 in LS – DYNA®). The simulations are done within a fully implicit setting.

Also, preliminary biaxial testing is done according to Wallmeier (2018) is presented in Appendix B.

The moisture ratio considered in the simulations are shown in Table 3.2

Table 3.2 Normalized moisture ratio at different humidity levels

Humidity level	*Normalized moisture ratio*
20 RH	0.69
50 RH	1
70RH	1.55
90 RH	2.39

[4] Execution time of a full sample is more because the stress state is not entirely uniaxial near the fixed end of the specimen.

[5] ELFORM – element formulation, refer LS-DYNA Keyword User's Manual I (2019) for more information

4 MODEL VERIFICATION

The proposed model is compared with the experimental results and the predefined material model in LS – DYNA®. Only few material models can be used to model paperboard in LS – DYNA®. The Xia – Nygårds model (Xia, Boyce, & Parks, 2002) is implemented as MAT 274 and it involves a lot of parameter extraction. Therefore, this model is not used for comparison with the proposed model.

The other model in LS – DYNA® that can be used for comparison is MAT 157 (LS-DYNA Keyword User's Manual II (2019)). This model is selected because of its simple but yet effective material treatment. The material is defined using anisotropic elasticity and isotropic hardening.

The flow stress is defined as

$$\sigma_Y = \sigma_{Y_0} + Q_{r1}\left(1 - \exp\left(-C_{r1}\varepsilon_{eff}^{p}\right)\right) + Q_{r2}\left(1 - \exp\left(-C_{r2}\varepsilon_{eff}^{p}\right)\right) \quad (4.1)$$

where σ_{Y_0} is the yield stress, σ_Y is the flow stress, ε_{eff}^{p} is the effective plastic strain, and $Q_{r1}, Q_{r2}, C_{r1}, C_{r2}$ are material parameters used to define the hardening behavior.

To make this model comparable with the implemented model, the hardening behavior should be linear. This can be done by assuming

$$Q_{r2} = 0; C_{r2} = 0 \; and C_{r1} \ll 0 \quad (4.2)$$

After expanding the exponential and only considering lower order terms

$$\sigma_Y = \sigma_{Y_0} + Q_{r1}C_{r1}\varepsilon_{eff}^{p} \quad (4.3)$$

which can be related to $H = Q_{r1}C_{r1}$; $C_{r1} \ll 0$.

Since the material model MAT 157 has isotropic hardening behavior, the same simulation cannot be used to model uniaxial specimens in both MD and CD. Thus, they are here modeled separately. This will not be the case for the proposed model because it can corporate different hardening moduli for different directions. The material card definitions used in LS-DYNA® are presented in detail in Appendix C.

4.1 CALIBRATION OF MATERIAL PARAMETERS FROM EXPERIMENTAL DATA

To implement the material model or use the MAT 157, the material constants defined in Section 3.1.1 and 3.1.2 have to be determined properly. The material constants at different moisture ratios are derived from the experiments performed by Marin. et al. (2020). The material constants evaluated for 50 % RH for both MD and CD directions are shown in Figure 4.1 and Figure 4.2.

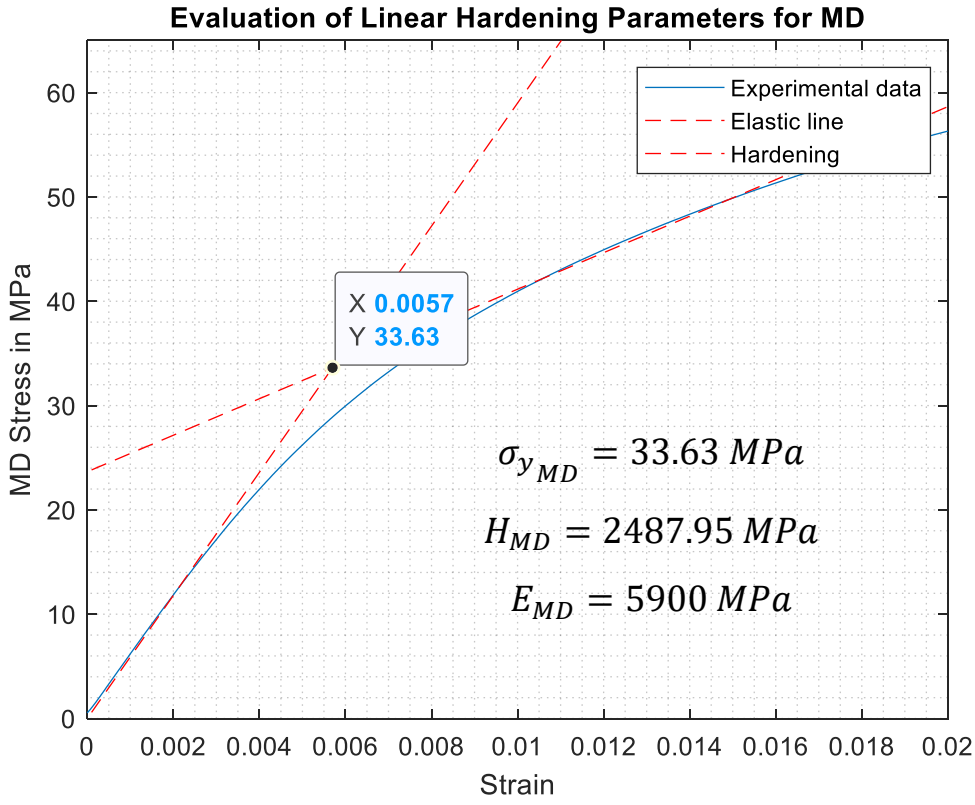

Figure 4.1 Evaluation of linear hardening parameters for MD at 50 % RH

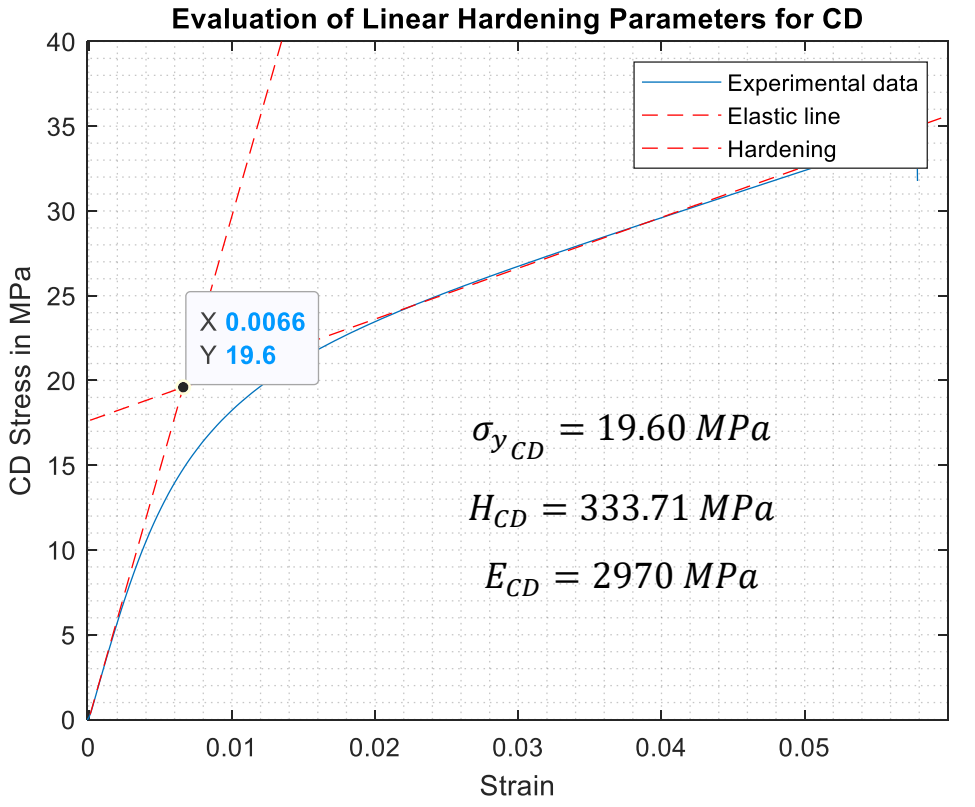

Figure 4.2 Evaluation of linear hardening parameters for CD at 50 % RH

The material constants for other humidity levels are evaluated using the same procedure that is used for MAT 157. For the proposed material model, the constants are evaluated using the relations presented in Section 2.2. The material parameters extracted for the both MD and CD directions are shown respectively in Table 4.1 and Table 4.2.

Table 4.1 Material Constants at all humidity levels for MD direction

Humidity Level	*Stiffness in MD (E_{MD}) (MPa)*		*Hardening Modulus in MD (H_{MD}) (MPa)*		*Yield Stress in MD (σ_{MD}^{y}) (MPa)*	
	Mean Experimental Evaluation	From the relation in Equation (2.1)	Mean Experimental Evaluation	From the relation in Equation (2.1)	Mean Experimental Evaluation	From the relation in Equation (2.1)
20 RH	**6700**	**6753.37**	**3030.43**	**2968.87**	**41.17**	**40.49**
50 RH	**5900**	**5900**	**2487.95**	**2487.95**	**33.63**	**33.63**
70 RH	**4800**	**4876.35**	**1976.50**	**2048.83**	**26.40**	**26.04**
90 RH	**2960**	**3042.63**	**1120.00**	**1150.79**	**10.64**	**11.92**

Table 4.2 Material Constants at all humidity levels for CD direction

Humidity Level	*Stiffness in CD (E_{CD}) (MPa)*		*Hardening Modulus in CD (H_{CD}) (MPa)*		*Yield Stress in CD (σ_{CD}^{y}) (MPa)*	
	Mean Experimental Evaluation	From the relation in Equation (2.1)	Mean Experimental Evaluation	From the relation in Equation (2.1)	Mean Experimental Evaluation	From the relation in Equation (2.1)
20 RH	**3450**	**3399.75**	**399.46**	**398.21**	**24.01**	**23.62**
50 RH	**2970**	**2970**	**333.71**	**333.71**	**19.60**	**19.60**
70 RH	**2400**	**2454.71**	**291.58**	**274.81**	**13.92**	**15.19**
90 RH	**1500**	**1531.63**	**174.82**	**154.27**	**6.552**	**6.958**

4.2 MODEL CHECKING IN MATLAB®

Before proceeding to the implementation of the material model in LS – DYNA®, a script for stress integration is developed in MATLAB®. A variety of tests ranging from single stress state to complete uniaxial testing is done. This is done to validate the material model and identify the mistakes before implementing it in LS – DYNA®.

Initially, things were made simpler by implementing ideal plasticity. The radial return method for a single stress state for Ideal plasticity is shown in Figure 4.3. The variation of residuals for the same is presented in Figure 4.4.

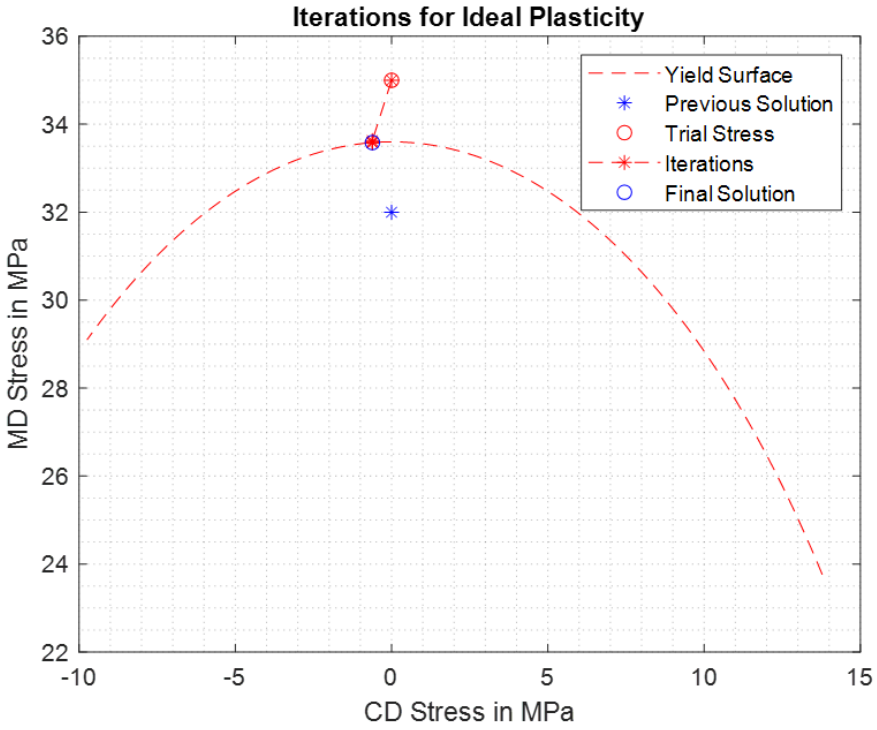

Figure 4.3 Radial Return method for ideal plasticity

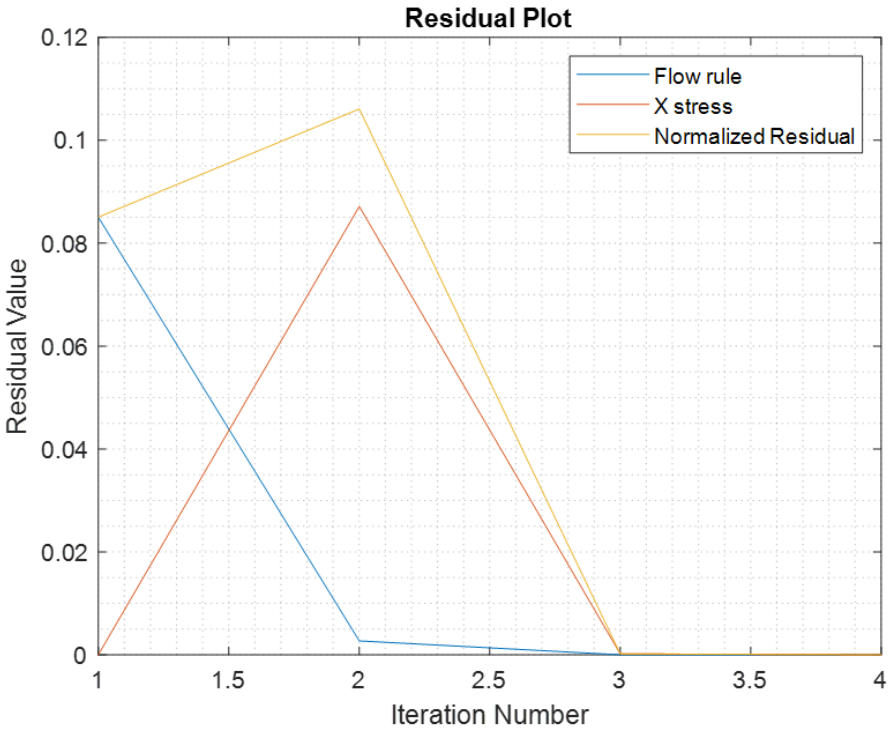

Figure 4.4 Residuals during iterations for ideal plasticity

Then the linear hardening is implemented and tested. The radial return method for a single stress state for linear hardening is shown in Figure 4.5. The variation of residuals for the same

analysis is presented in Figure 4.6. All samples tested are initially done with uniaxial testing in MD and later CD has been verified.

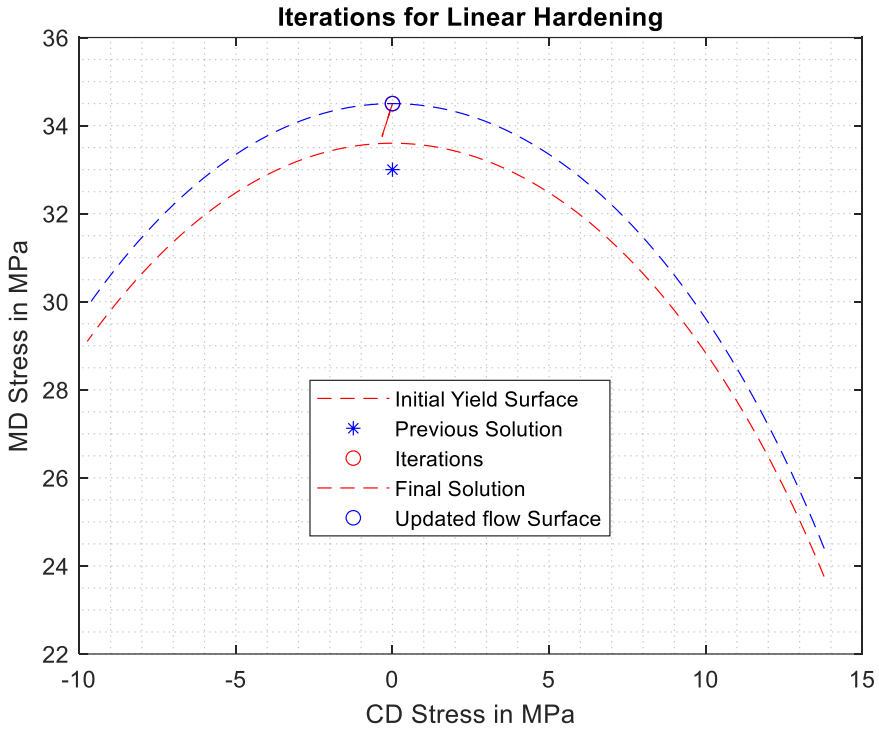

Figure 4.5 Radial return method for linear hardening

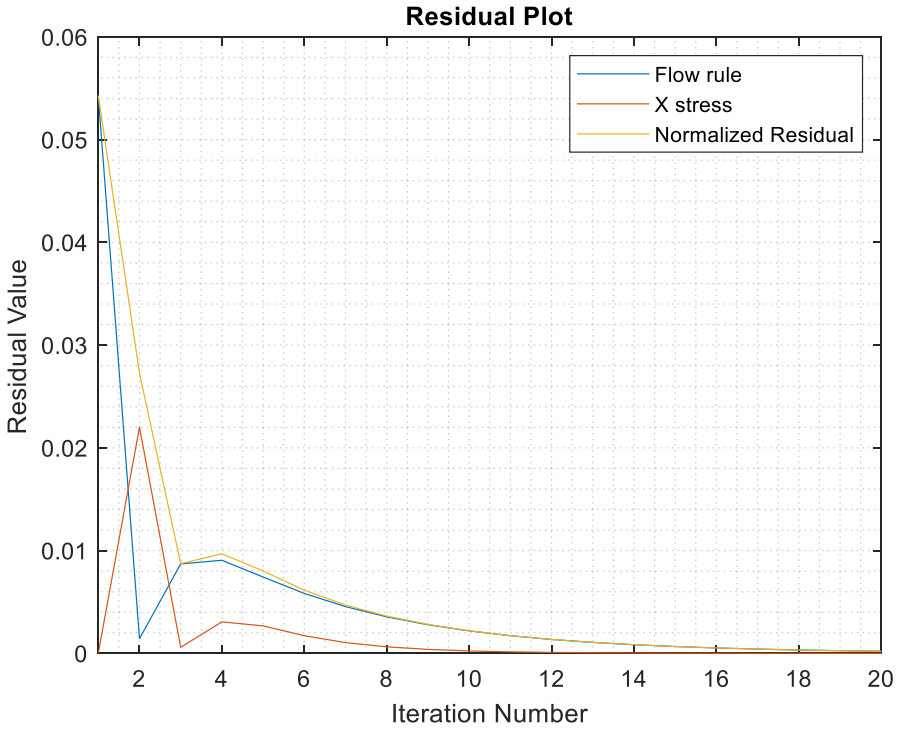

Figure 4.6 Residuals during iterations for linear hardening

Then a full – scale testing is done in MATLAB® to validate the stress integration technique for a complete uniaxial testing. This is done by assuming an elastic stress state and then the radial return method is applied in a loop. After finishing one loop, an elastic stress state is assumed and then the algorithm for stress integration was applied.

The different stress states from only elastic, ideal plasticity and linear hardening are shown in Figure 4.7.

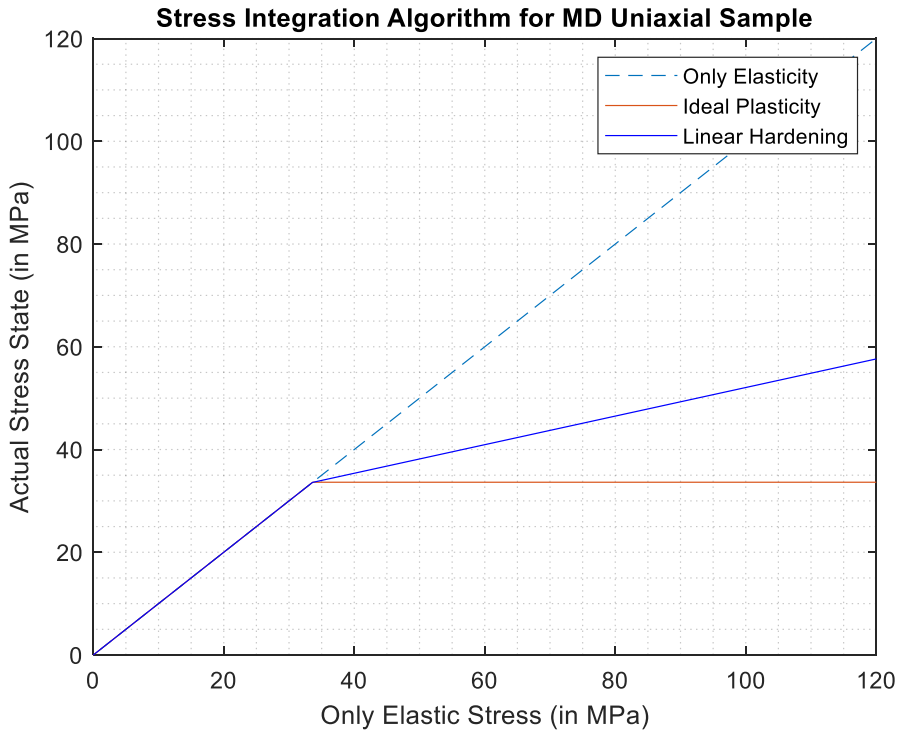

Figure 4.7 Stress integration algorithm implemented in MATLAB® for MD uniaxial sample

The same results have been compared to the experimental data by considering an equivalent displacement for the solution in MATLAB®. This is usually computed using the tangent stiffness in any commercial finite element software.

The comparison between experimental data and the proposed anisotropic linear hardening model for MD uniaxial sample is shown in Figure 4.8. The same comparison for a CD uniaxial sample is shown in Figure 4.9.

A section of residuals during the simulation for a MD uniaxial sample with linear hardening is shown in Figure 4.10. The X-axis in the figure represents the cumulative iteration number in the entire simulation.

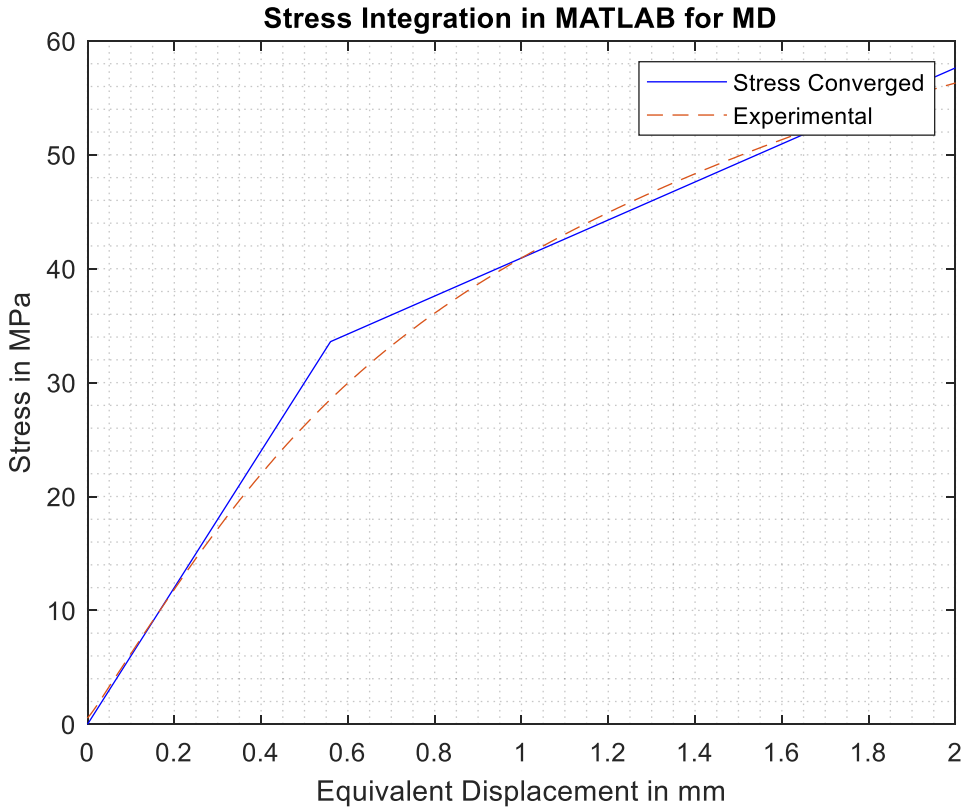

Figure 4.8 Stress response curve for MD sample in MATLAB®

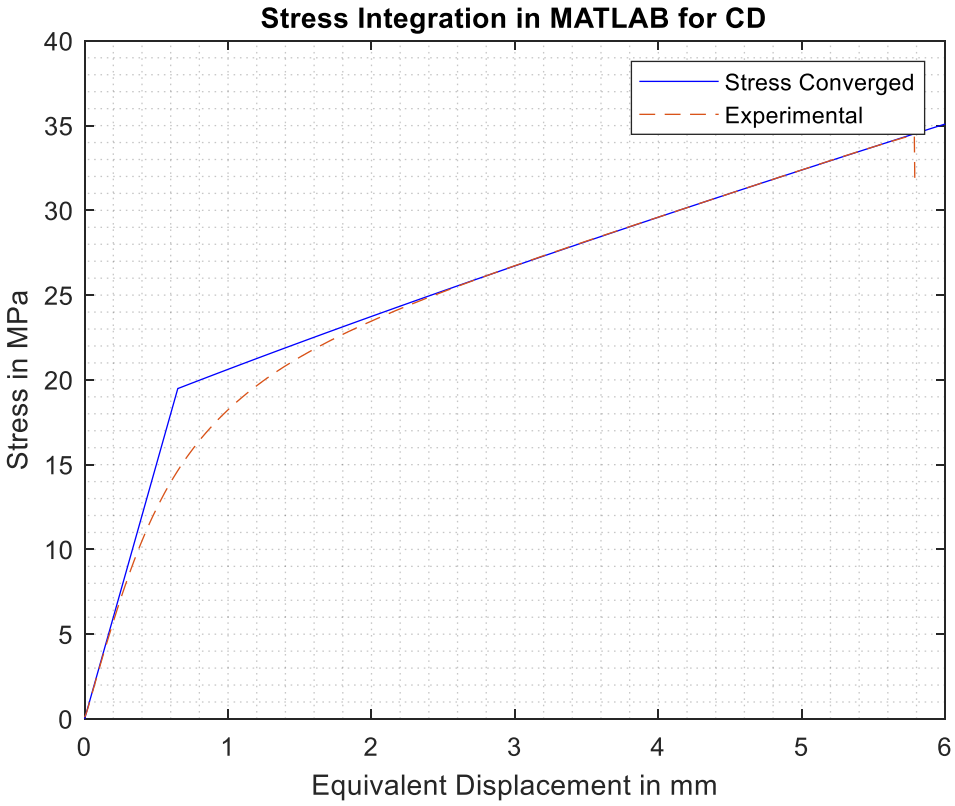

Figure 4.9 Stress response curve for CD sample in MATLAB®

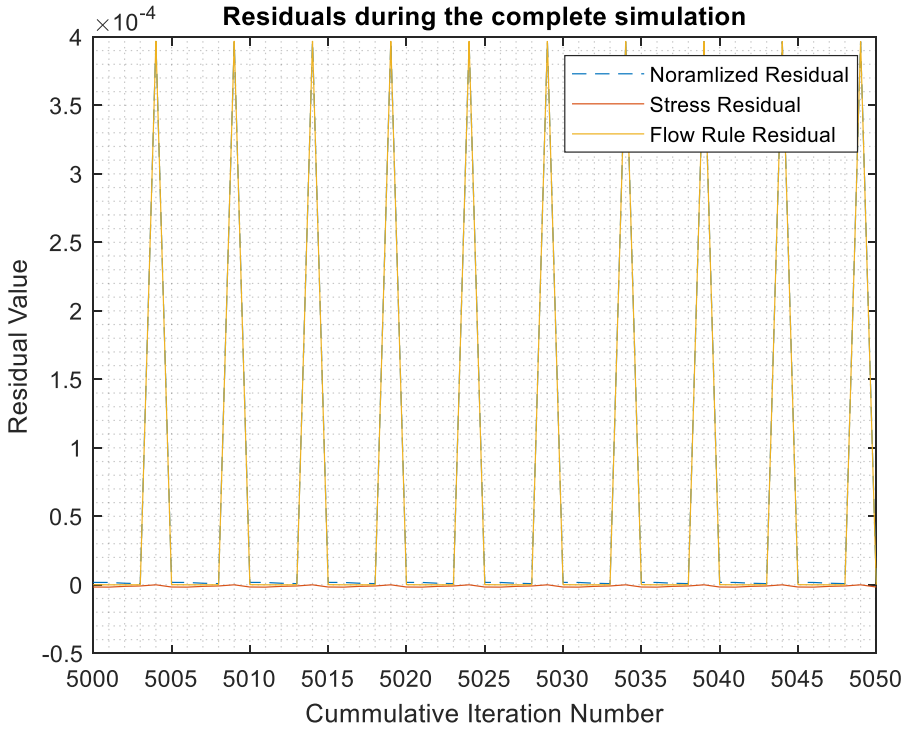

Figure 4.10 Residuals during the complete simulation

4.3 FOUR ELEMENT SIMULATION IN LS-DYNA®

After successful evaluation of stress integration in MATLAB®, small-scale simulation is setup in LS-DYNA. It is done by modelling a structure consisting of four identical quadratic elements of side 1 mm. The model with boundary conditions are shown in Figure 4.11.

The complete algorithm presented in Table 3.1 is implemented in a stepwise manner in LS-DYNA. Initially only elasticity is assumed and scripted in LS-DYNA. Thereafter, moisture scaling of the elastic constants is done. This is presented for a CD uniaxial sample in Figure 4.12. Then the yield condition is implemented with ideal plasticity.

After successful implementation of ideal plasticity, the complete model with anisotropic hardening and with moisture scaling is implemented. This is presented for a CD uniaxial sample in Figure 4.13.

Since the stress state in the sample is uniaxial, the results for both MD and CD should match with the corresponding MAT 157 simulations. The MD sample results for both MAT 157 and proposed model is shown in Figure 4.14. The CD sample results for both MAT 157 and proposed model is shown in Figure 4.15.

These simulations are done with fully integrated shell (ELFORM 2 in LS-DYNA®) and solid elements (ELFORM 16 in LS-DYNA®). The simulations are done in an implicit setting.

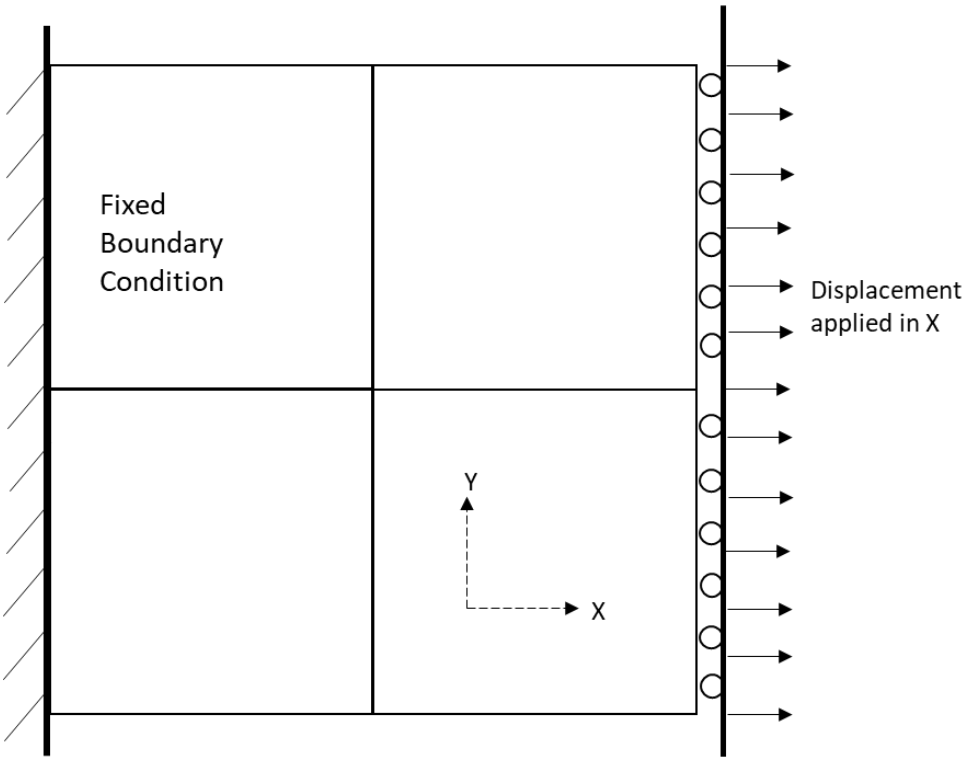

Figure 4.11 Four Element sample modelled in LS-DYNA

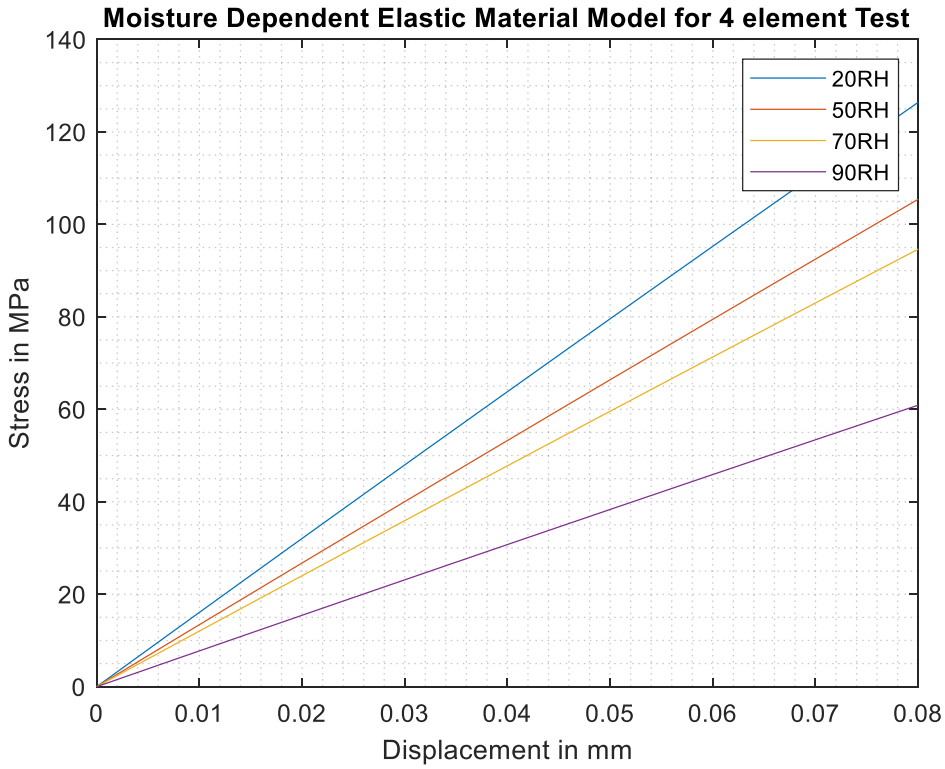

Figure 4.12 Moisture dependent elastic response in LS - DYNA for 4 element test at different humidity levels

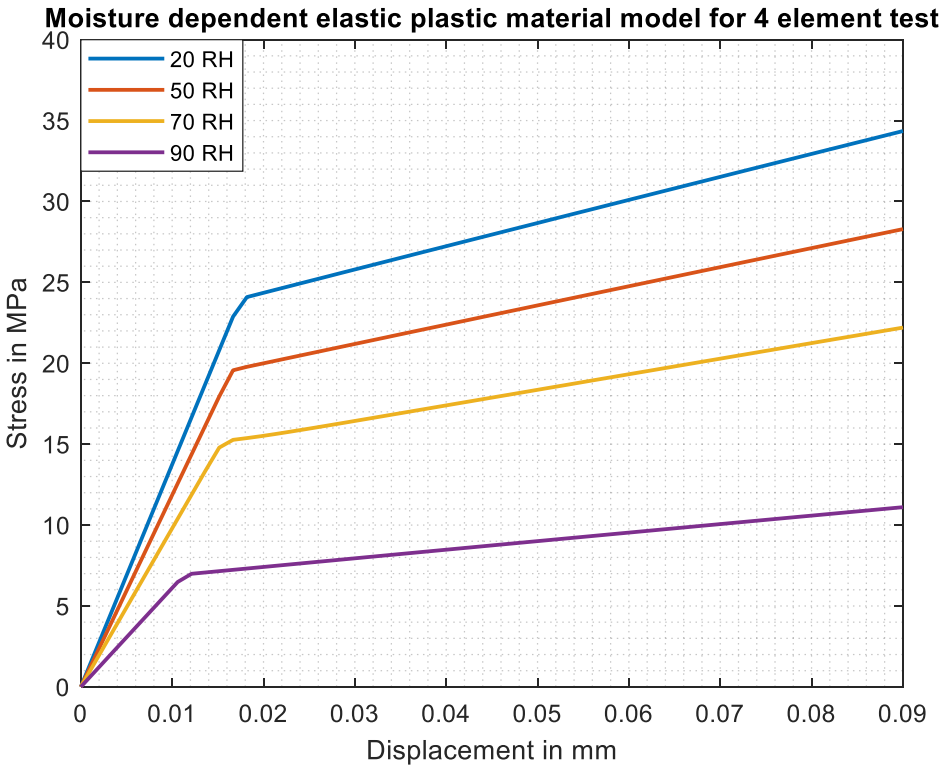

Figure 4.13 Moisture dependent elastic plastic response in LS - DYNA for 4 element test at different humidity levels

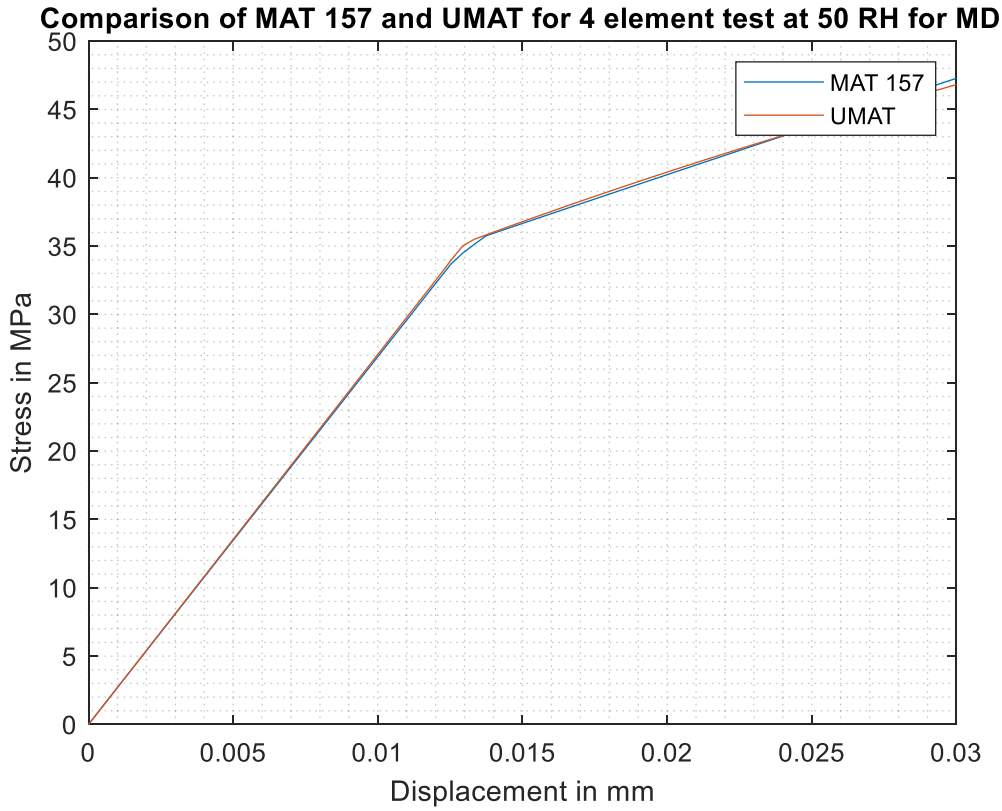

Figure 4.14 Comparison of material models for four-element MD sample at 50 RH

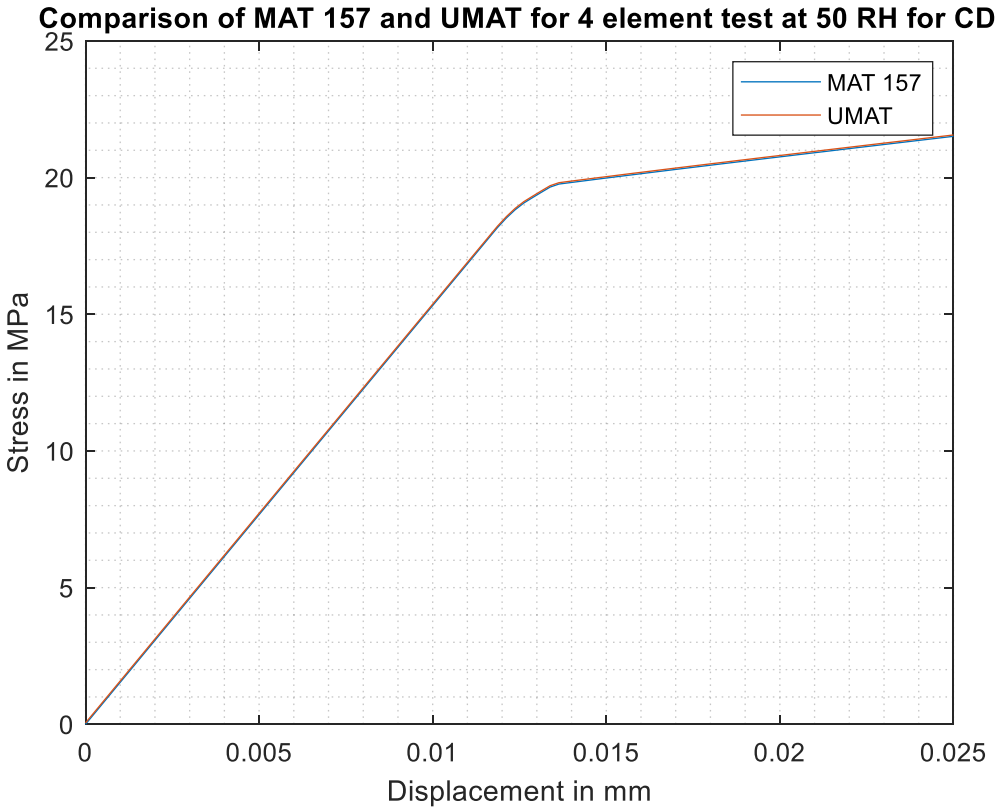

Figure 4.15 Comparison of material models for four-element CD sample at 50 RH

5 RESULTS

The simulations are done for both MAT 157 and the proposed model for both MD and CD samples at different humidity levels. The simulation results for MD and CD samples at the normal humidity level of 50 % RH are shown, respectively in Figure 5.1 and Figure 5.2.

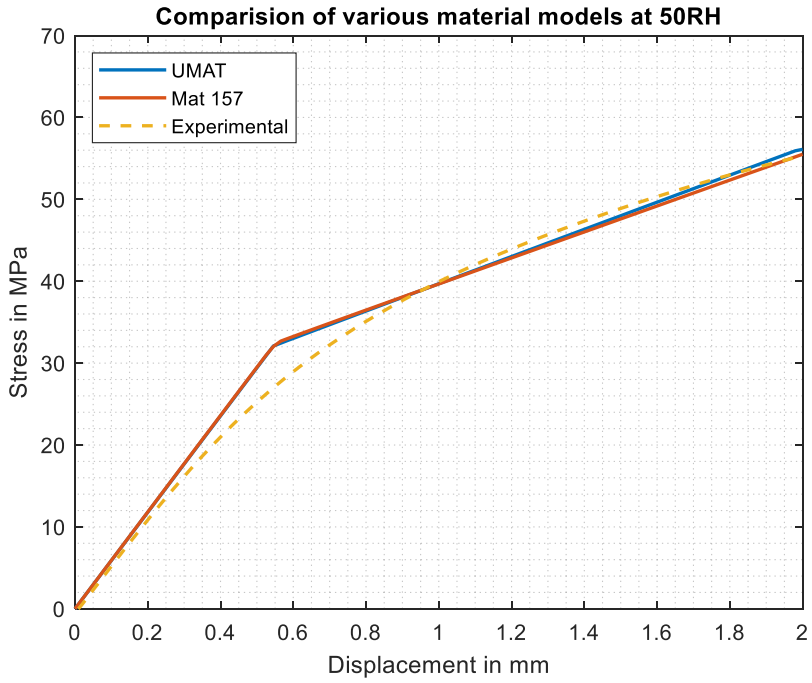

Figure 5.1 Stress response curve for an MD uniaxial specimen at 50 % RH

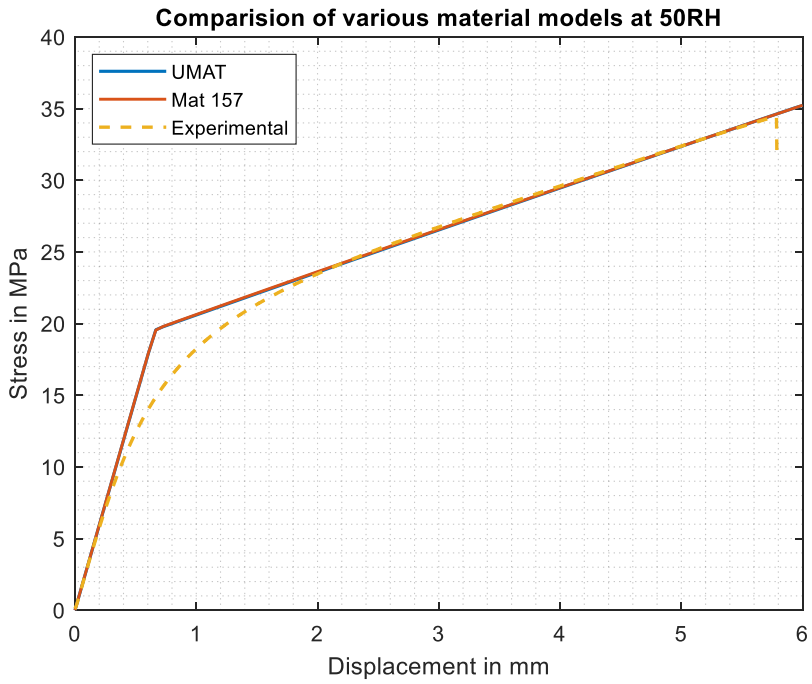

Figure 5.2 Stress response curve for a CD uniaxial specimen at 50 % RH

Similarly, all simulations for MD and CD samples are done at different humidity levels. The results from them are shown respectively, in Figure 5.3 and Figure 5.4.

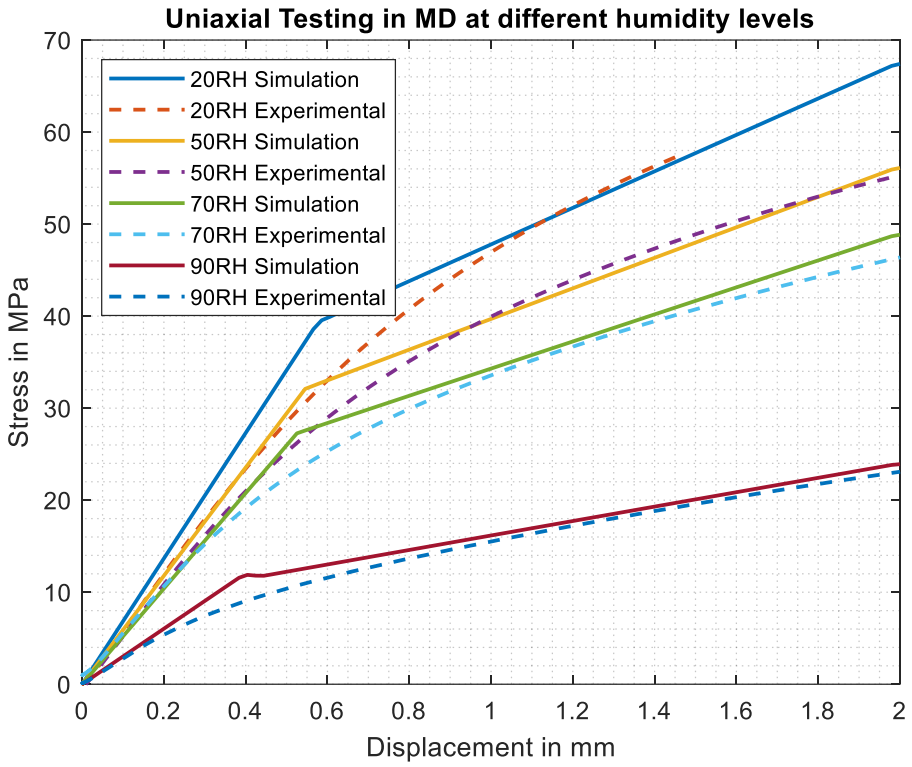

Figure 5.3 Stress response curve for an MD uniaxial specimen at all humidity levels

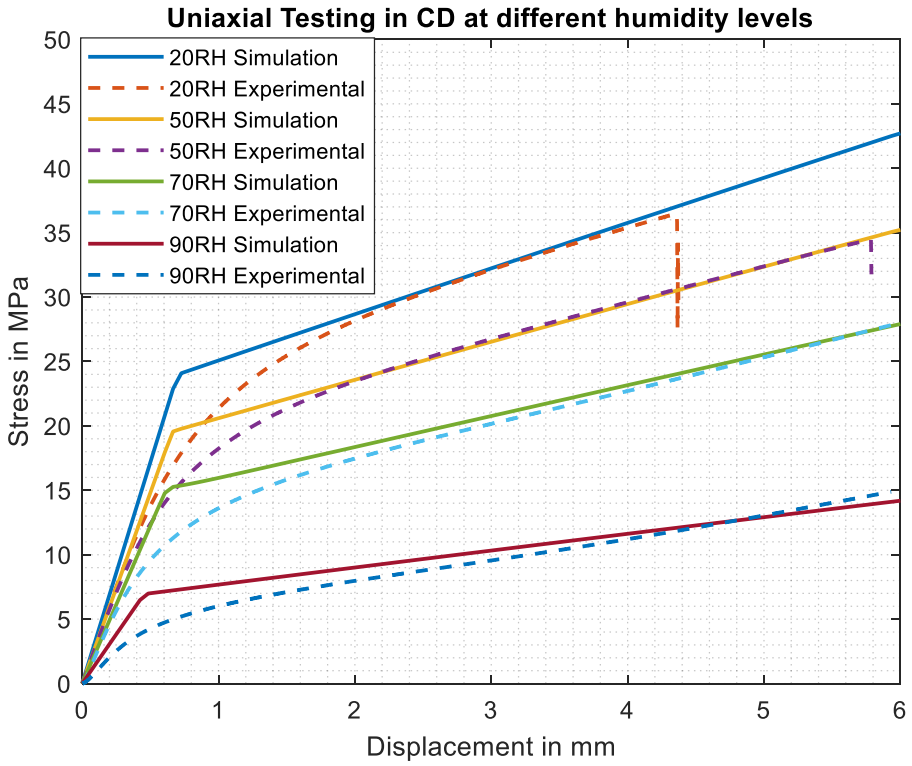

Figure 5.4 Stress response curve for a CD uniaxial specimen at all humidity levels

6 DISCUSSION

Element selection in LS – DYNA

Shell elements are traditionally used to model paperboard. The shell elements can capture the strains in the thickness direction better than the solid elements. If solid element is modeled for out of plane problems, there must be a number of solid elements in the thickness direction to get an efficient solution. This makes the computation more complex and the simulation is more prone to the locking phenomenon. The other elements, which are better for out-of-plane problems are solid shell elements. They are named as TSHELL in LS – DYNA®. Since the simulations are in – plane, the results will not vary much for shell and solid elements. All the simulations are done in implicit mode, so fully integrated elements are used. They are shell: ELFORM 2 in LS – DYNA® and solid: ELFORM 16 in LS – DYNA®.

Issues in LS – DYNA:

For any orthotropic material, the material axes needed to be defined properly for an accurate simulation. These are defined in differ ways for shells and solids in LS – DYNA refer Keyword User's manual II (2019). The method employed in all of the simulations is that the material axes are rotated to achieve the required material direction. In LS – DYNA® one vector is needed to define material axes for shells whereas two vectors are needed for solids. While using shell elements (with the same method as used in MAT 157 to define material axes) in coupling with UMAT, many null rows of the stiffness matrix occurred. The same did not occur when the UMAT was used for solid elements. Upon investigation, it was found that when using shell elements, the element direction[6] is taken as the material direction for computation. This problem can be solved for uniaxial samples but could not be solved for biaxial sample because of the geometry. Therefore, to avoid confusion all the simulations using UMAT are done with solid elements.

Uniaxial Results

The comparison of the results has been done with averaged experimental data. This can be a problem in assessing the results, since the relations between material parameters and moisture ratio are computed using all the samples. The linear hardening approximation looks better for stress response in CD than MD. The moisture scaling was accurate enough at humidity level of 20 RH for both CD and MD. For humidity level of 70 % RH, the yield stress drifted from the fitted linear response for both MD and CD. The drifting was more for the CD sample. However, the hardening followed more or less the same for both MD and CD. At the humidity level of 90 % RH where all the things start being deviated, even the elastic response was a bit off. This can be attributed to low value of the coefficient of determination (R^2) for the yield stress and hardening modulus when compared to the elastic stiffness.

[6] Element direction in shell: The X axis is defined as the vector defined by the direction from local element node 1 to 2

7 CONCLUSION AND RECOMMENDATIONS

7.1 SUMMARY OF WORK DONE

A new material model is proposed for paperboard to model the in-plane response at different humidity levels. The model comprises of orthotropic elasticity and anisotropic linear hardening. All the mechanical parameters are considered functions of moisture ratio. An implicit variant of this model is implemented in LS-DYNA®. All necessary checks are done in MATLAB® before implementing the material model in LS-DYNA®. A step-by-step procedure is used while implementing the material model in LS-DYNA®. A small-scale model is tested initially and used for debugging. Then uniaxial simulations are done on the experimental specimens and the results were verified with the experimental results. The results were found to be in acceptable agreement for both the MD and CD simulations. Finally, it should be noted that the thermodynamic consistency of the proposed model and its implementation in LS-Dyna has not been verified. This is not expected to be a problem for the pre-dominantly uniaxial simulation results presented here, but could possibly be of concern for the biaxial simulations presented in Appendix B.

7.2 FUTURE RECOMMENDATIONS

Different fitting procedures for moisture scaling

The relation between moisture ratio and material parameters can be changed to a higher order (or exponential fit) to get the coefficient of determination (R^2) close to unity. In tandem to that, confidence bounds to the fitted relations can also be determined. This makes the fitting procedure more robust and can be useful to modeling the variations in paper. The basic idea is shown in Figure 7.1.

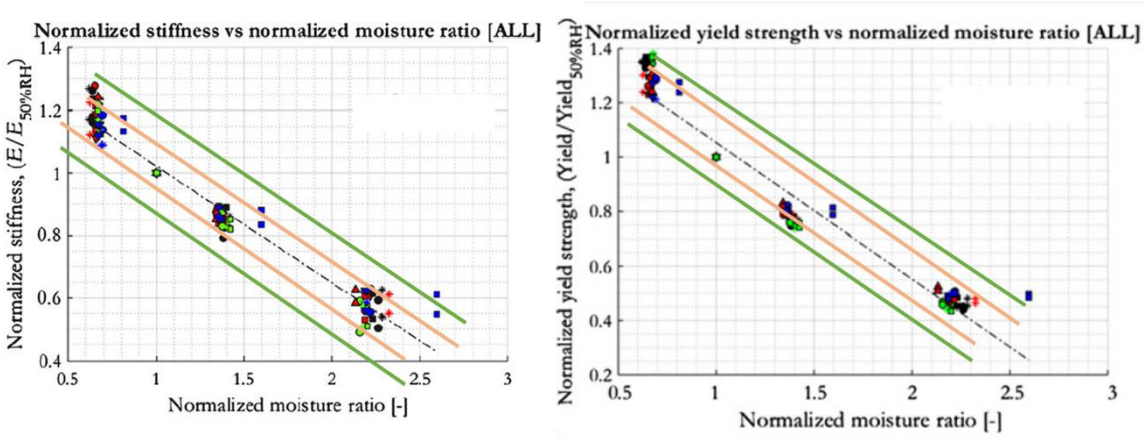

Figure 7.1 Relation between stiffness and yield strength with moisture ratio including confidence bounds

The orange lines in the Figure 7.1 covers some of the sample points, whereas the green line covers almost all of the sample points. There is also limitation to this type of fitting procedure since many more samples are needed to predict the correct bounds.

Introduce kinematic hardening

Here, the paperboard is assumed to have the same mechanical properties in compression and tension, which gives a poor estimate in biaxial simulations. This problem can be solved by adding kinematic hardening to the already defined anisotropic hardening. Then the complete material model includes anisotropic and kinematic hardening, which can be used to solve many relevant problems.

To define kinematic hardening, the definition of back stress becomes necessary. This definition can add some more parameters as described by Borgqvist, .et.al (2014). Kinematic hardening without any additional variables is defined in Tjahjanto, .et. al.(2015). This definition can be used in addition to the already defined model.

Changes can be made to the Equation (3.6) to implement kinematic hardening as

$$f = \frac{\sigma_i^2 + \sigma_{b_i}^2}{\left(\sigma_i^s(m_r)\right)^2} = 1 \tag{7.1}$$

where σ_{b_i} is the introduced back stress. The back stress should correspond to the previous loading direction. That means that it should be history dependent.

In Tjahjanto, .et. al.(2015), the back stress is assumed to be

$$\tau_b^{(\alpha)} = s_a^{(\bar{\alpha})} \tag{7.2}$$

where $\bar{\alpha}$ indicates the sub-yield surface opposite to surface α. Consequently, no additional parameter is required to describe the evolution of the back stress. However, in the present model being considered here, there are no sub-surfaces. In this scenario, it can be assumed that

$$\begin{aligned} \sigma_{b_{MD}} &= H_{CD} \frac{\partial f}{\partial \sigma_{CD}} \lambda \\ \sigma_{b_{CD}} &= H_{MD} \frac{\partial f}{\partial \sigma_{MD}} \lambda \end{aligned} \tag{7.3}$$

where $\sigma_{b_{MD}}$, $\sigma_{b_{CD}}$ are the back stresses defined in MD and CD respectively, H_{MD}, H_{CD} are the linear hardening moduli and, λ is the effective plastic strain.

The other four stress components can be tricky to identify. As a start, this material model can be implemented, and other complexities can be further added.

Moisture ratio as a state variable

This project assumed that moisture ratio is a boundary condition, but to model the moisture changes in an uncontrolled environment properly, the moisture ratio has to be considered as a state variable. In making moisture a state variable, the strain due to change in moisture also need to be considered. By defining the strain due to moisture change, a moisture evolution law is needed as similar to plastic flow rule evolution. This can be done by assuming moisture ratio as a function of all other state variables: stress state, incremental effective plastic strain, and the environmental variables.

$$m_r = f\left(\sigma_{ij}, \Delta\lambda_n, m_r^{env}\right) \tag{7.4}$$

This function can be evaluated by conducting experiments in an uncontrolled environment. During these experiments, the weight of the sample has also to be measured in parallel stress and strain. This can help in deducing the moisture content of the sample during the whole testing. This information can be used to fit a curve with the other state variables.

By introducing this function, the values, which are assumed zero while calculating much of the stuff in Sections 3.2.1 and 3.2.2 cannot be zero. They should instead be computed using the Equation (7.4)

$$\frac{\partial m_r}{\partial \sigma_k} \neq 0 \; ; \frac{\partial m_r}{\partial(\Delta\lambda_n)} \neq 0; dm_r \neq 0$$

This also introduces a new variable in the system of equations, and they become indeterminant. Thus, an extra equation is needed to make them determinant. The extra equation in this case is the ***diffusion equation***. This equation in addition to the system of equations defined in Section 3.2.1 can be used to identify the next iteration values. This also makes the tangent stiffness more complicated and necessary care must be taken to evaluate the differentials.

By introducing moisture ratio as a state variable, changes in moisture can be modeled. To model mechanosorptive creep, there is also a need for a term accelerating the strain due to moisture changes.

8 REFERENCES

Barg, P., & Oskar, L. (2019, August 7). *Pulp, paper, and packaging in the next decade: Transformational change*. (Mckinsey & Company) Retrieved from https://www.mckinsey.com/industries/paper-forest-products-and-packaging/our-insights/pulp-paper-and-packaging-in-the-next-decade-transformational-change

Baum, G., Brennan D, C., & Habeger, C. (1981). Orthotropic elastic constants of paper. *Tappi Journal, 64*(8), 97-101.

Bonet, J., & Wood, R. (1997). *Nonlinear continuum mechanics for finite element analysis* (2nd ed.). Cambridge: Cambridge University Press.

Borgqvist, E., Lindström, T., Tryding, J., Wallin, M. & Ristinmaa, M. (2014). Distortional hardening plasticity model for paperboard,. *International Journal of Solids and Structures, 51*(13), 2411-2423,.

Borodulina, S., Kulachenko, A., Galland, S., & Nygårds, M. (2012). Stress-strain curve of paper revisited. *Nordic Pulp and Paper Research Journal, 27*(2), 318-328.

Erhart, T. (2010). An overview of user-defined interfaces in LS-DYNA. *9th LS-DYNA Forum.* Bamberg: Dynamore GmbH.

Erkkilä, A.-L., Leppänen, T., & Hämäläinen, J. (2013). Empirical plasticity models applied for paper sheets having different anisotropy and dry solids content levels. *International Journal of Solids and Structuures, 50*(14-15), 2151-2179.

Gudmundson, P. (2010). *Material Mechanics.* Stockholm: Department of Solid Mechanics, KTH Engineering Sciences.

Gustafsson, P. & Niskanen, K. (2012). Paper as an engineering material. In *Mechanics of paper products,* K. Niskanen (Ed.) (pp. 4-26). Berlin: De Guyter.

Harrysson, M., & Ristinmaa, M. (2007). Description of evolving anisotropy at large strains. *Mechanics of Materials, 39*(3), 267-282.

Huang, H., & Nygårds, M. (2010). A simplified material model for finite element analysis of paperboard creasing. *Nordic Pulp and Paper Research Journal, 25*(4), 505-512.

Khodayari, A. (2020, January 2). *Fibernet*. Retrieved from http://fibrenet.eu/index.php?id=blog-post-31

Kulachenko, A. (2012). Moisture Induced Deformations. In In *Mechanics of paper products,* K. Niskanen (Ed.) (pp. 163-180). Berlin: De Gruyter.

Li, P., Guo, Y. & Shim, V. (2018). A constitutive model for transversely isotropic material with anisotropic hardening. *International Journal of Solids and Structures, 138*, 40-49.

Linvill, E., Wallmeier, M., & Östlund, S. (2017). A constitutive model for paperboard including wrinkle prediction and post-wrinkle behavior applied to deep drawing,. *International Journal of Solids and Structures,, 117*, 143-158.

Liu, C., Huang, Y. & Stout, M. G. (1997). On the asymmetric yield surface of plastically orthotropic materials: A phenomenological study. *Acta Materialia, 45*(6), 2397-2406.

Livermore Software Technology Corporation (LSTC). (2019). *LS-DYNA® Keyword User's Manual Volume I.* Livermore.

Livermore Software Technology Corporation (LSTC). (2019). *LS-DYNA® Keyword User's Manual Volume II.* Livermore.

Marin, G., Nygårds, M., & Östlund, S. (2020). Elastic-plastic model for the mechanical properties of paperboard as a function of moisture. *Nordic Pulp and Paper Research Journal*, doi.org/10.1515/npprj-2019-0104.

Motamedian, H. R. & Kulachenko, A. (2019). Simulating the hygroexpansion of paper using a 3D beam network model and concurrent multiscale approach,. *International Journal of Solids and Structures, 161*, 23-41.

Nygårds, M. (2005). *3DM Three dimensional finite element modelling of paperboard.* Stockholm: STFI-Packforsk.

Nygårds, M. (2008). Experimental techniques for characterization of elasticplastic material properties in paperboard. *Nordic Pulp and Paper Research Journal, 23*(4), 432-437.

Pfeiffer, M., & Kolling, S. (2019). A non-associative orthotropic plasticity model for paperboard under in-plane loading. *International Journal of Solids and Structures, 166*, 112-113.

Tjahjanto, D., Girlanda, O. & Östlund, S. (2015). Anisotropic viscoelastic–viscoplastic continuum model for high-density cellulose-based materials. *Journal of the Mechanics and Physics of Solids, 84*, 1-20.

Wallmeier, M. (2018). *Benchmark studies for the simulation of paperboard forming.* Stockholm.

Wallmeier, M., Linvill, E., Hauptmann, M., Majschak, J.-P., & Östlund, S. (2015). Explicit FEM analysis of the deep drawing of paperboard. *Mechanics of Materials, 89*, 202-215.

Wikipedia. *Paper*. Retrieved from Wikipedia Free Encyclopedia: https://en.wikipedia.org/wiki/Paper

Xia, Q. S., Boyce, M. C. & Parks, D. M. (2002). A constitutive model for the anisotropic elastic–plastic deformation of paper and paperboard,. *International Journal of Solids and Structures,, 39*(15), 4053-4071,.

Zienkiewicz, O., Taylor, R., & Zhu, J. (2013). *The Finite Element Method.* Butterworth-Heinemann.

APPENDIX A MATERIAL MODEL

A.1 DEFINITION OF INCREMENTAL PLASTIC STRAIN

The plastic strain increment can be written as

$$d\epsilon_k^p = d\lambda \left.\frac{\partial f}{\partial \sigma_k}\right|_n^i$$

$$\frac{\partial f}{\partial \sigma_k} = \frac{\partial}{\partial \sigma_k}\left(\sum_{k=1}^{6} \frac{\sigma_k^2}{\left(\sigma_k^y(m_r) + H_k(m_r)\epsilon_k^p\right)^2} - 1\right)$$

$$\Rightarrow \frac{\partial f}{\partial \sigma_k} = \frac{2\sigma_k}{\left(\sigma_k^y(m_r) + H_k(m_r)\epsilon_k^p\right)^2} - \frac{H_k\sigma_k^2 \frac{d\epsilon_k^p}{d\sigma_k}}{\left(\sigma_k^y(m_r) + H_k(m_r)\epsilon_k^p\right)^3}$$

And it is known that from the definition of hardening modulus

$$H_k = \frac{d\sigma_k}{d\epsilon_k^p} \Rightarrow H_k \frac{d\epsilon_k^p}{d\sigma_k} = 1$$

Substituting this the equation changes to

$$\frac{\partial f}{\partial \sigma_k} = \frac{2\sigma_k}{\left(\sigma_k^y(m_r) + H_k(m_r)\epsilon_k^p\right)^2} - \frac{\sigma_k^2}{\left(\sigma_k^y(m_r) + H_k(m_r)\epsilon_k^p\right)^3}$$

To find the plastic strain increment for a particular direction substitute this gradient and integrate it

$$\Delta\epsilon_k^{p,n} = \int_{\lambda_n}^{\lambda_{n+1}} \left(\frac{2\sigma_k}{\left(\sigma_k^{y,n}(m_r) + H_k(m_r)\epsilon_k^{p,n}\right)^2} - \frac{\sigma_k^2}{\left(\sigma_k^{y,n}(m_r) + H_k(m_r)\epsilon_k^{p,n}\right)^3}\right) d\lambda$$

To make the model simple, this gradient can be assumed as a constant in the integral bounds, which give the incremental plastic strain as

$$\Delta\epsilon_k^{p,n} = \left(\frac{2\sigma_k}{\left(\sigma_k^{s,n}(m_r)\right)^2} - \frac{\sigma_k^2}{\left(\sigma_k^{s,n}(m_r)\right)^3}\right)\Delta\lambda_n$$

$$\sigma_k^{s,n} = \sigma_k^{y,n}(m_r) + H_k(m_r)\epsilon_k^{p,n} \; ; flow\ stress\ at\ n^{th} time\ step$$

This is the one that has been implemented in the model. So, this makes the model dependent on the size of incremental effective plastic strain. This has to be small to make sure that the model converges.

To make it independent of the size of incremental plastic strain, the integral must be evaluated assuming the gradient is not constant. This can be done by the general definition of plastic strain in that direction as

$$\epsilon_k^p = \frac{2\sigma_k}{(\sigma_k^s)^2}\,\lambda = \mathrm{X}_k\lambda$$

Substituting this in the integral,

$$\Delta\epsilon_k^{p,n} = \int_{\lambda_n}^{\lambda_{n+1}} \left(\frac{2\sigma_k}{\left(\sigma_k^y + H_k \mathrm{X}_k \lambda\right)^2} - \frac{\sigma_k^2}{\left(\sigma_k^y + H_k \mathrm{X}_k\,\lambda\right)^3} \right) d\lambda \;; Let\; H_k \mathrm{X}_k = \Gamma_k$$

Changing the integral domains

$$\Rightarrow \Delta\epsilon_k^{p,n} = \int_0^{\Delta\lambda_n} \left(\frac{2\sigma_k}{\left(\sigma_k^{s,n} + \Gamma_k^n \lambda\right)^2} - \frac{\sigma_k^2}{\left(\sigma_k^{s,n} + \Gamma_k^n\,\lambda_k\right)^3} \right) d\lambda$$

$$\Rightarrow \Delta\epsilon_k^{p,n} = -\frac{2\sigma_k}{\Gamma_k\left(\sigma_k^{s,n} + \Gamma_k^n\lambda\right)} - \frac{\sigma_k^2}{\Gamma_k\left(\sigma_k^{s,n} + \Gamma_k^n\lambda\right)^2}\Bigg|_0^{\Delta\lambda_n}$$

$$\Rightarrow \quad -\frac{2\sigma_k}{\Gamma_k\left(\sigma_k^{s,n} + \Gamma_k^n\Delta\lambda_n\right)} - \frac{\sigma_k^2}{\Gamma_k\left(\sigma_k^{s,n} + \Gamma_k^n\Delta\lambda_n\right)^2} + \frac{2\sigma_k}{\Gamma_k^n\sigma_k^{s,n}} + \frac{\sigma_k^2}{\Gamma_k^n\left(\sigma_k^{s,n}\right)^2}$$

$$\because \Gamma_k^n = H_k \mathrm{X}_k^n = \frac{H_k 2\sigma_k}{\left(\sigma_k^{s,n}\right)^2}$$

$$\Rightarrow \frac{1}{H_k} + \frac{\sigma_k}{2H_k\sigma_k^{s,n}} - \left[\frac{\sigma_k^{s,n}}{H_i\left(\sigma_k^{s,n} + \Gamma_k^n\Delta\lambda_n\right)}\right] - \frac{\sigma_k\sigma_k^{s,n}}{H_i\left(\sigma_k^{s,n} + \Gamma_k^n\Delta\lambda_n\right)^2}$$

$$\Rightarrow \Delta\epsilon_k^{p,n} = \frac{1}{H_k}\left[1 - \frac{\sigma_k^{s,n}}{\sigma_k^{s,n} + \Gamma_k^n\Delta\lambda_n}\right] + \frac{\sigma_k}{2H_k}\left[\frac{1}{\sigma_k^{s,n}} - \frac{\sigma_k^{s,n}}{\left(\sigma_k^{s,n} + \Gamma_k^n\Delta\lambda_n\right)^2}\right]$$

$$\Rightarrow \Delta\epsilon_k^{p,n} = \frac{1}{H_k}\left[\frac{\Gamma_k^n\Delta\lambda_n}{\sigma_k^{s,n+1}}\right] + \frac{\sigma_k}{2H_k}\left[\frac{(\Gamma_k^n\Delta\lambda_n)^2 + 2\sigma_k^{s,n}\Gamma_k^n\Delta\lambda_n}{\sigma_k^{s,n}\left(\sigma_k^{s,n+1}\right)^2}\right]$$

$$\Rightarrow \Delta\epsilon_k^{p,n} = \frac{2\sigma_k\Delta\lambda_n}{\left(\sigma_k^{s,n}\right)^2\sigma_k^{s,n+1}} + \frac{\sigma_k^2}{\left(\sigma_k^{s,n}\right)^2}\left[\frac{\Gamma_k^n\Delta\lambda_n^2 + 2\sigma_k^{s,n}\Delta\lambda_n}{\sigma_k^{s,n}\left(\sigma_k^{s,n+1}\right)^2}\right]$$

$$\Rightarrow \Delta\epsilon_k^{p,n} = \frac{2\sigma_k\Delta\lambda_n}{\left(\sigma_k^{s,n}\right)^2\sigma_k^{s,n+1}} + \frac{2\sigma_k^3 H_k\Delta\lambda_n^2}{\sigma_k^{s,n}\left(\sigma_k^{s,n+1}\right)^2} + \frac{2\sigma_k^2\Delta\lambda_n}{\left(\sigma_k^{s,n}\right)^2\left(\sigma_k^{s,n+1}\right)^2}$$

$$\Rightarrow \Delta\epsilon_k^{p,n} = \left[\frac{2\sigma_k}{\left(\sigma_k^{s,n}\right)^2\sigma_k^{s,n+1}} + \frac{2\sigma_k^2}{\left(\sigma_k^{s,n}\right)^2\left(\sigma_k^{s,n+1}\right)^2}\right]\Delta\lambda_n + \left(\frac{2\sigma_k^3 H_k}{\sigma_k^{s,n}\left(\sigma_k^{s,n+1}\right)^2}\right)\Delta\lambda_n^2$$

A.2 JACOBIAN IN NEWTON RAPHSON METHOD

The Jacobian $\frac{dF}{dx}$ in the Newton – Raphson can be written as

$$\bar{F}_{ik} = \frac{\partial F_i}{\partial \sigma_k} = \delta_{ik} + 2\,\Delta\lambda_n \frac{d}{d\sigma_k}\left(\frac{C_{ij}(m_r)\sigma_j}{\left(\sigma_j^{s,n}(m_r)\right)^2}\right) - 2\,\Delta\lambda_n \frac{d}{d\sigma_k}\left(\frac{C_{ij}(m_r)\sigma_j^2}{\left(\sigma_j^{s,n}(m_r)\right)^3}\right); i,k = 1,..,6$$

The plastic increment is a variable here, so it is not considered as a function of the stress state and vice – versa.

$$\Rightarrow \bar{F}_{ik} = \delta_{ik} + 2\,\Delta\lambda_n \left[\frac{\partial C_{ij}}{\partial m_r}\frac{\partial m_r}{\partial \sigma_k}\frac{\sigma_j}{\left(\sigma_j^{s,n}(m_r)\right)^2} - 2\frac{C_{ij}(m_r)\sigma_j}{\left(\sigma_j^{s,n}(m_r)\right)^3}\frac{\partial \sigma_j^{s,n}}{\partial m_r}\frac{\partial m_r}{\partial \sigma_k} + \frac{C_{ij}(m_r)\frac{d\sigma_j}{d\sigma_k}}{\left(\sigma_j^{s,n}(m_r)\right)^2}\right]$$
$$- 2\,\Delta\lambda_n \left[\frac{\partial C_{ij}}{\partial m_r}\frac{\partial m_r}{\partial \sigma_k}\frac{\sigma_j^2}{\left(\sigma_j^{s,n}(m_r)\right)^3} - 3\frac{C_{ij}(m_r)\sigma_j}{\left(\sigma_j^{s,n}(m_r)\right)^4}\frac{\partial \sigma_j^{s,n}}{\partial m_r}\frac{\partial m_r}{\partial \sigma_k}\right.$$
$$\left. + \frac{2C_{ij}(m_r)\sigma_j\frac{d\sigma_j}{d\sigma_k}}{\left(\sigma_j^{s,n}(m_r)\right)^3}\right]$$

In this model, the moisture ratio is considered to be a boundary condition rather than a state variable. So, the gradient of moisture ratio with the state variables both stress state and incremental plastic strain are considered to be zero

$$\frac{\partial m_r}{\partial \sigma_k} = 0\,; \frac{\partial m_r}{\partial(\Delta\lambda_n)} = 0$$

$$\Rightarrow \bar{F}_1 = \bar{F}_{ik} = \delta_{ik} + 2\,\Delta\lambda_n D_{ij}\delta_{jk} - 4\,\Delta\lambda_n E_{ij}\delta_{jk}$$
$$\Rightarrow \bar{F}_1 = \bar{F}_{ik} = \delta_{ik} + [2\,D_{ik} - 4E_{ik}\sigma_k]\Delta\lambda_n; i,k = 1,..,6 \qquad \text{(A.1)}$$

The same gradient with the incremental effective plastic strain can be written as

$$\bar{F}_2 = \bar{F}_{i7} = \frac{\partial F_i}{\partial(\Delta\lambda_n)}$$

$$\Rightarrow \bar{F}_{i7} = 2\frac{\boldsymbol{C}_{ij}\sigma_j}{\left(\sigma_j^{s,n}\right)^2} + 2\left[\frac{\frac{\partial \boldsymbol{C}_{ij}}{\partial m_r}\sigma_j}{\left(\sigma_j^{s,n}\right)^2} + \frac{\boldsymbol{C}_{ij}\frac{\partial \sigma_j}{\partial m_r}}{\left(\sigma_j^{s,n}\right)^2} - \frac{2\boldsymbol{C}_{ij}\sigma_j}{\left(\sigma_j^{s,n}\right)^3}\frac{\partial \sigma_j^{s,n}}{\partial m_r}\right]\frac{\partial m_r}{\partial(\Delta\lambda_n)} - 2\frac{\boldsymbol{C}_{ij}\sigma_j^2}{\left(\sigma_j^{s,n}\right)^3}$$
$$- 2\left[\frac{\frac{\partial \boldsymbol{C}_{ij}}{\partial m_r}\sigma_j^2}{\left(\sigma_j^{s,n}\right)^3} + \frac{2\boldsymbol{C}_{ij}\sigma_j\frac{\partial \sigma_j}{\partial m_r}}{\left(\sigma_j^{s,n}\right)^2} - \frac{3\boldsymbol{C}_{ij}\sigma_j^2}{\left(\sigma_j^{s,n}\right)^4}\frac{\partial \sigma_j^{s,n}}{\partial m_r}\right]\frac{\partial m_r}{\partial(\Delta\lambda_n)}$$

$$\because \frac{\partial m_r}{\partial(\Delta\lambda_n)} = 0 \Rightarrow \bar{F}_2 = \bar{F}_{i7} = 2D_{ij}\sigma_j - 2E_{ij}\sigma_j^2 \; ; i = 1,..,6 \tag{A.2}$$

The gradient of the flow rule with the stress state is given as

$$\bar{F}_3 = \bar{F}_{7k} = \frac{\partial F_7}{\partial \sigma_k}$$

$$= 2\frac{\sigma_k}{\left(\sigma_k^{s,n} + H_k \Delta\epsilon_i^P\right)^2}$$

$$- 2\left(\sum_{i=1}^{6}\left[\frac{\sigma_i^2}{\left(\sigma_i^{s,n} + H_i\,\Delta\epsilon_i^P\right)^3}\frac{\partial\sigma_i^{s,n}}{\partial m_r} + \Delta\lambda_n\left[\frac{\sigma_i^2}{\left(\sigma_i^{s,n} + H_i\,\Delta\epsilon_i^P\right)^3}\frac{\partial H_i}{\partial m_r}\right]\right]\right)\frac{\partial m_r}{\partial \sigma_k}$$

$$\because \frac{\partial m_r}{\partial \sigma_k} = 0 \; \bar{F}_3 = \bar{F}_{7k} = \frac{\partial F_7}{\partial \sigma_k} = \frac{2\sigma_k}{\left(\sigma_k^{s,n} + H_k\,\Delta\epsilon_i^P\right)^2} \; ; k = 1,2,3,4,5,6 \tag{A.3}$$

The same with the incremental effective plastic strain can be written as

$$\bar{F}_4 = \bar{F}_{77} = \frac{\partial F_7}{\partial(\Delta\lambda_n)}$$

$$= -2\left(\sum_{i=1}^{6}\left[\frac{\sigma_i^2 H_i\,\frac{d\Delta\epsilon_i^P}{d\Delta\lambda_n}}{\left(\sigma_i^{s,n} + H_i\,\Delta\epsilon_i^P\right)^3}\right.\right.$$

$$\left.\left. + \left[\frac{\sigma_i^2}{\left(\sigma_i^{s,n} + H_i\,\Delta\epsilon_i^P\right)^3}\frac{\partial\sigma_i^{s,n}}{\partial m_r} + \Delta\lambda_n\left(\frac{\sigma_i^2}{\left(\sigma_i^{s,n} + H_i\Delta\epsilon_i^P\right)^3}\frac{\partial H_i}{\partial m_r}\right)\right]\right]\right)\frac{\partial m_r}{\partial(\Delta\lambda_n)}$$

From the associative plasticity, it is known that

$$\Delta\epsilon_i^p = \Delta\lambda_n \left.\frac{\partial f}{\partial\sigma_i}\right|_n = \Delta\epsilon_i^p = \Delta\lambda_n \frac{2\sigma_i}{\left(\sigma_i^{s,n}\right)^2} \Rightarrow \frac{d\Delta\epsilon_i^p}{d\Delta\lambda_n} = \frac{2\sigma_i}{\left(\sigma_i^{s,n}\right)^2} \; , \because \frac{\partial m_r}{\partial(\Delta\lambda_n)} = 0$$

$$\Rightarrow \bar{F}_4 = \bar{F}_{77} = \frac{\partial F_7}{\partial(\Delta\lambda_n)} = -4\sum_{i=1}^{6}\frac{\sigma_i^3 H_i}{\left(\sigma_i^{s,n} + H_i\Delta\epsilon_i^P\right)^3\left(\sigma_i^{s,n}\right)^2} \tag{A.4}$$

Finally, from the Equations (A.1-A.4), the Jacobian $\frac{dF}{dx}$ in matrix form can be written as

$$\frac{dF}{dx} = \bar{F}_{ik} = \begin{bmatrix}[\bar{F}_1]_{6\times6} & [\bar{F}_2]_{6\times1}\\ [\bar{F}_3]_{1\times6} & [\bar{F}_4]_{1\times1}\end{bmatrix} \tag{A.5}$$

From Equations A.1 – A.5, the incremental plastic strain and the stress state for the next state are evaluated for newton Raphson.

A.3 ALGORITHMIC TANGENT STIFFNESS

The Equations (3.36) and (3.37) are the system of equations used in evaluating the stress state and incremental plastic strains. They are

$$\begin{aligned} &\left[\delta_{ij} + 2D_{ij}\Delta\lambda_n\right]\sigma_j - 2E_{ij}\sigma_j^2\Delta\lambda_n = \bar{\sigma}_i \; ; \; \bar{\sigma}_i = C_{ij}\varepsilon_j \\ &f\left(\sigma_i, \Delta\lambda_n, \sigma_i^s(m_r), H_i(m_r)\right) = \sum_{i=1}^{6}\left[\frac{\sigma_i}{\sigma_i^{s,n} + H_i\,\Delta\epsilon_i^p}\right]^2 - 1 = 0 \end{aligned} \tag{A.6}$$

Now differentiating the first equation

$$\begin{aligned} d\sigma_i = {} & dC_{ij}\epsilon_j + C_{ij}d\epsilon_j - \left[2D_{ij}\sigma_j - 2E_{ij}\sigma_j^2\right]d\Delta\lambda_n \\ & - \left[2\left(D_{ij}d\sigma_j + dD_{ij}\sigma_j\right) - 4\left(E_{ij}\sigma_j d\sigma_j + dE_{ij}\sigma_j^2\right)\right]\Delta\lambda_n \end{aligned} \tag{A.7}$$

$$dD_{ij} = \frac{\partial D_{ij}}{\partial m_r}dm_r \quad dE_{ij} = \frac{\partial E_{ij}}{\partial m_r}dm_r \; dC_{ijkl} = \frac{\partial C_{ij}}{\partial m_r}dm_r$$

$$\because dm_r = 0 \Rightarrow dD_{ij} = dE_{ij} = dC_{ij} = 0 \tag{A.8}$$

Substituting Equation A.8 in A.7

$$\Rightarrow \left(\delta_{ij} + \left[2D_{ij} + 4E_{ij}\sigma_j\right]\Delta\lambda_n\right)d\sigma_j = C_{ij}d\epsilon_j - \left[2D_{ij}\sigma_j + 2E_{ij}\sigma_j^2\right]d(\Delta\lambda_n) \tag{A.9}$$

The only unknown in Equation A.9 is $d(\Delta\lambda_n)$. It can be written in terms of $d\sigma_{ij}$ using the flow rule and consistency condition. The consistency condition states that

$$\lambda\dot{f} = 0 \Rightarrow df = 0 \; \because \lambda \neq 0$$

Where df is the total derivate of the flow rule which can be written as

$$df = \sum_{i=1}^{6}\frac{\partial f}{\partial\sigma_i}d\sigma_i + \frac{\partial f}{\partial(\Delta\lambda_n)}d(\Delta\lambda_n) + \sum_{i=1}^{6}\left[\frac{\partial f}{\partial\sigma_i^s}\frac{\partial\sigma_i^s}{\partial m_r} + \frac{\partial f}{\partial H_i}\frac{\partial H_i}{\partial m_r}\right]dm_r = 0$$

$$\Rightarrow df = \sum_{i=1}^{6}\frac{\partial f}{\partial\sigma_i}d\sigma_i + \frac{\partial f}{\partial(\Delta\lambda_n)}d(\Delta\lambda_n) = 0 \because dm_r = 0$$

$$\Rightarrow d(\Delta\lambda_n) = -\frac{\sum_{i=1}^{6}\frac{\partial f}{\partial\sigma_i}d\sigma_i}{\frac{\partial f}{\partial(\Delta\lambda_n)}} = -\frac{(\nabla f_{n+1}^T)^i d\sigma}{\frac{\partial f}{\partial(\Delta\lambda_n)}} \tag{A.10}$$

$(\nabla f_{n+1}^T)^i = \left[\frac{\partial f}{\partial\sigma_1} \quad \cdots \quad \frac{\partial f}{\partial\sigma_6}\right]$ is the gradient of flow rule with the stress state

Substituting Equation A.10 in A.9 gives the Equation (3.38)

$$\left(\delta_{ij} + \left[2D_{ij} + 4E_{ij}\sigma_j\right]\Delta\lambda_n\right)d\sigma_j = C_{ij}d\epsilon_j + \left[2D_{ij}\sigma_j + 2E_{ij}\sigma_j^2\right]\frac{(\nabla f_{n+1}^T)^i d\sigma}{\left(\frac{\partial f}{\partial(\Delta\lambda_n)}\right)} \tag{A.11}$$

APPENDIX B BIAXIAL TESTING

B.1 BIAXIAL SPECIMEN

The biaxial testing is one of the main benchmarks to validate a user-defined material model for paperboard. The biaxial simulation done is the benchmark problem 1 of (Wallmeier, Benchmark studies for the simulation of paperboard forming, 2018). The geometry is simplified by only modeling one quarter of the sample using symmetry boundary conditions is shown in Figure B.1.

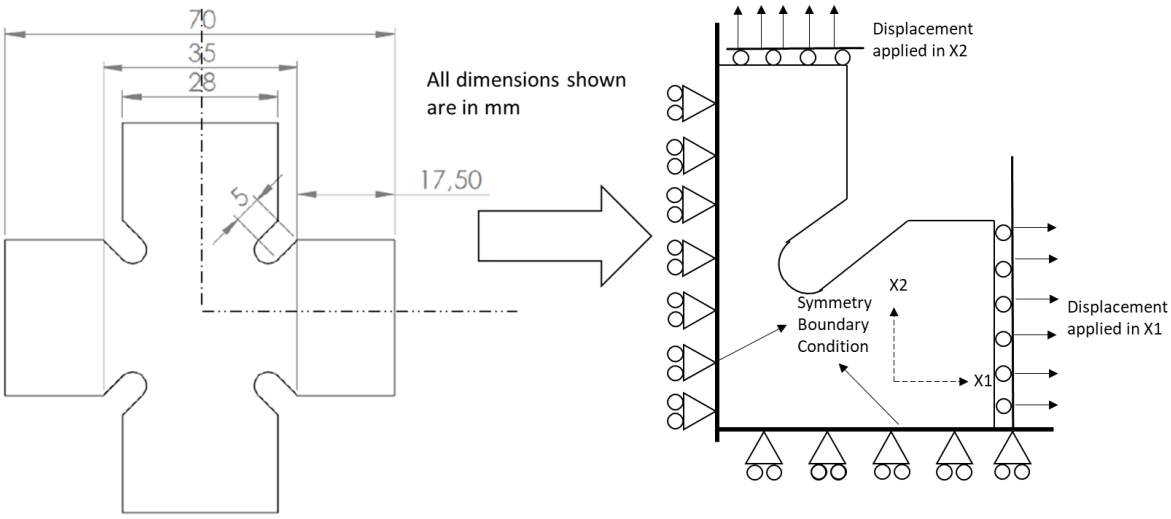

Figure B.1 Geometry of biaxial sample and finite element model

This sample is modeled using shell elements for MAT 157 and it is modeled using solid elements for the UMAT. The loading is applied as displacement on the green lines shown in Figure B.1.

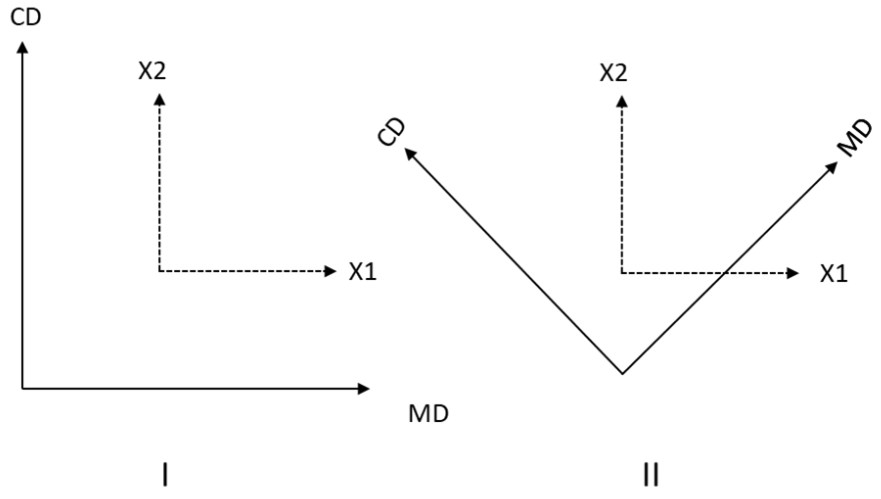

Figure B.2 Material axes and loading axes definitions for both simulations

Two simulations are done for every humidity level

I. Test 1: The material axes of the sample MD and CD coincide with the corresponding axes X1 and X2 (shown in Figure B.1).
II. Test 2: The material axes of the sample make an angle of 45^{o} with the axes X1 and X2 (shown in Figure B.1).

They are shown in Figure B.2.

Since MAT 157 has only isotropic hardening, the yield stress and hardening modulus for test 1 and test 2 are considered to the normalized components of both MD and CD values. The hardening for UMAT was not considered (see Section B.4).

The loading conditions also vary for the two tests and they are presented in Table B.1.

Table B.1 Loading conditions of biaxial sample for both test cases

Time in s	*Loading Axis*	*Displacement in mm*		*Resultant Displacement*
		Test 1	*Test 2*	
0 – 1	X1	**0.1**	**0.1**	Tension
	X2	**0.4**	**0.3**	Tension
2.4 – 3.4	X1	**0.3**	**0.3**	Tension
	X2	**0.2**	**0.2**	Compression
4.8 – 5.8	X1	**0.2**	**0.2**	Compression
	X2	**0.5**	**0.4**	Tension

All simulations are done with a fully integrated shell (ELFORM 2 in LS – DYNA®) for MAT 157 and solid elements (ELFORM 16 in LS – DYNA®) for UMAT.

The following results are of interest as mentioned in Wallmeier (2018).

- The Force response curve in both directions at both clamps
- The x and y displacement of the point *'P'* specified in Figure B.3.

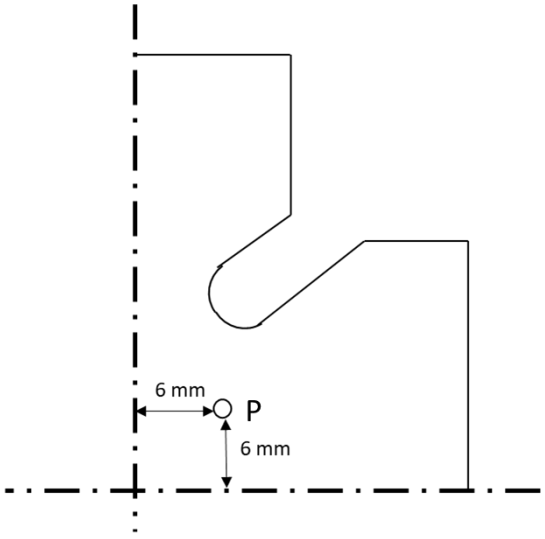

Figure B.3 Point definition for displacement measurement

B.2 BIAXIAL TEST 1

The displacements of the point *'P'* for both material models at 50 % RH is shown in Figure B.4. The same for 20 % RH is shown in Figure B.5.

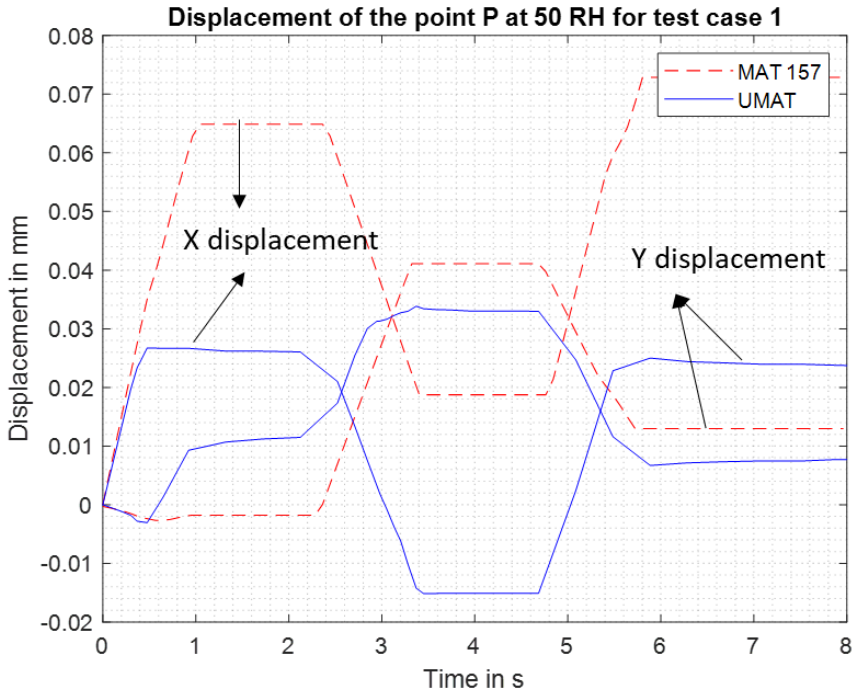

Figure B.4 Displacement of point P at 50 % RH for test case 1

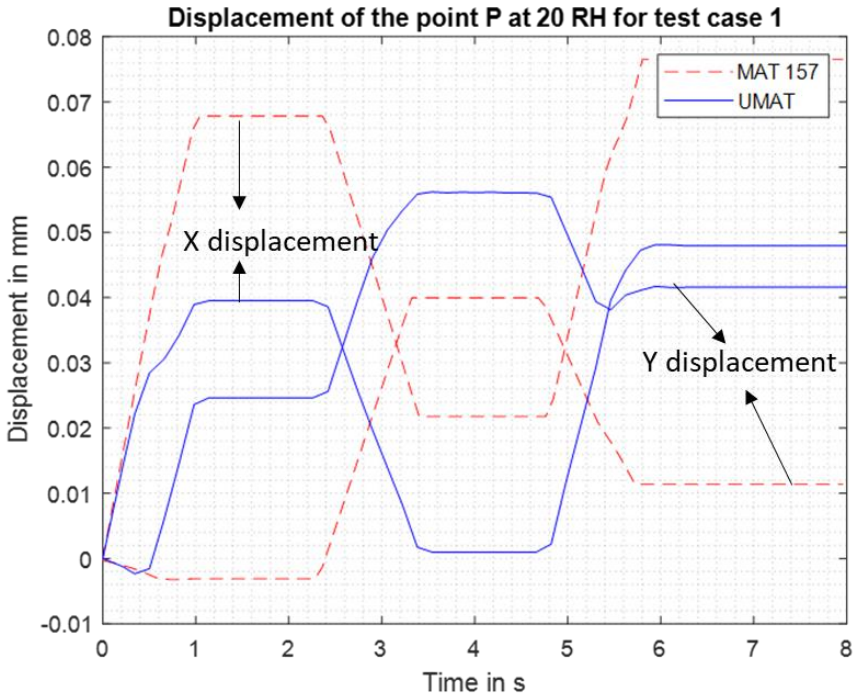

Figure B.5 Displacement of point P at 20 % RH for test case 1

The force response curve for 50 % RH and 20 % RH are shown respectively in Figure B.6 and Figure B.7.

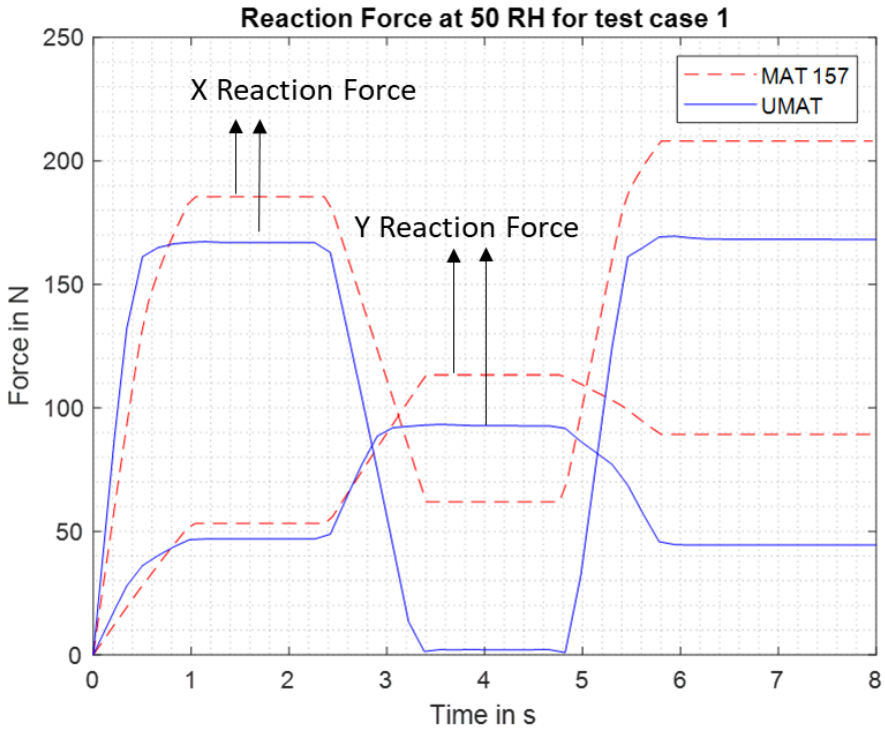

Figure B.6 Reaction forces at clamps at 50 % RH for test case 1

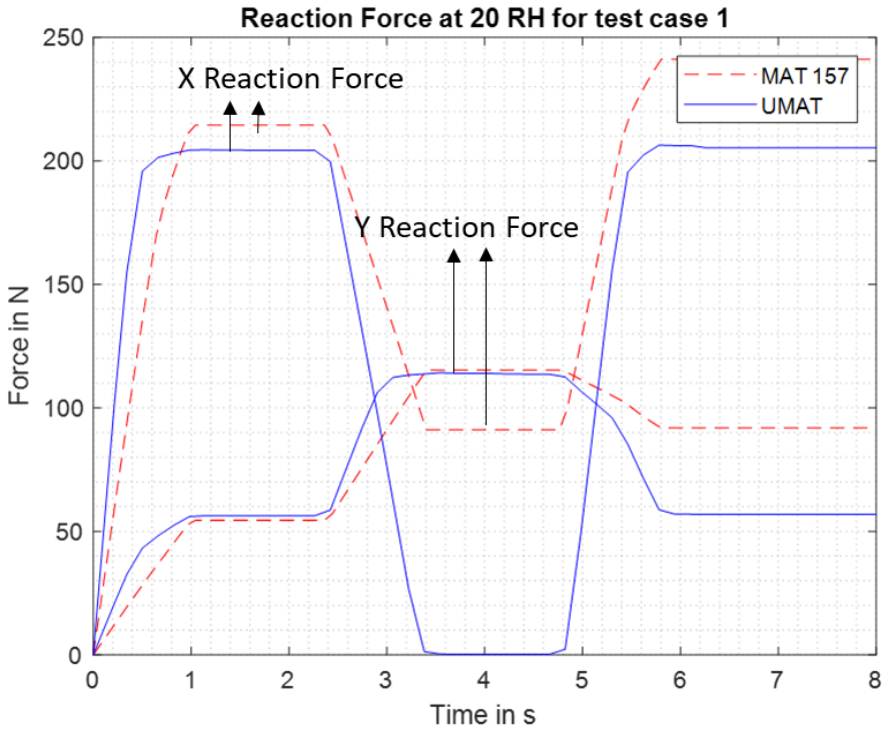

Figure B.7 Reaction forces at clamps at 20 % RH for test case 1

B.3 BIAXIAL TEST 2

The displacements of the point *'P'* for both material models at 50 % RH is shown in Figure B.8. The same for 20 % RH is shown in Figure B.9.

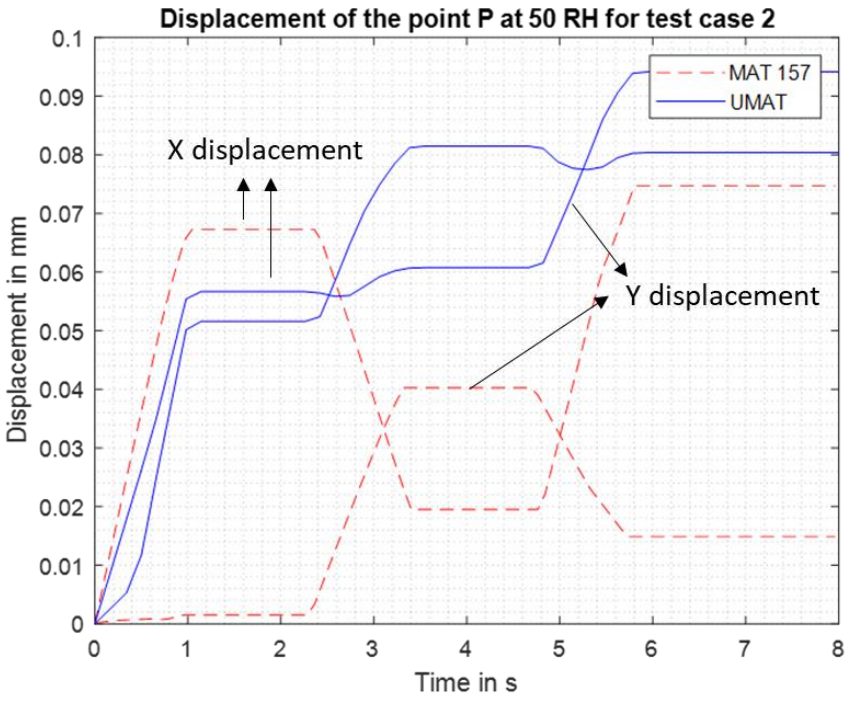

Figure B.8 Displacement of point P at 50 % RH for test case 2

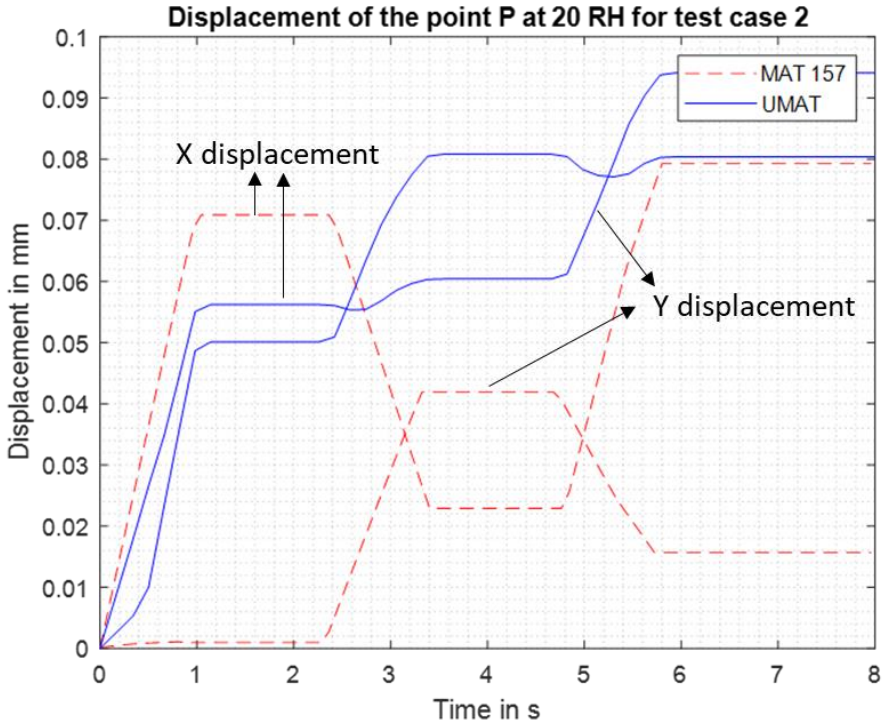

Figure B.9 Displacement of point P at 20 % RH for test case 2

The force response curve for 50 % RH and 20 % RH are shown respectively in Figure B.10, Figure B.11.

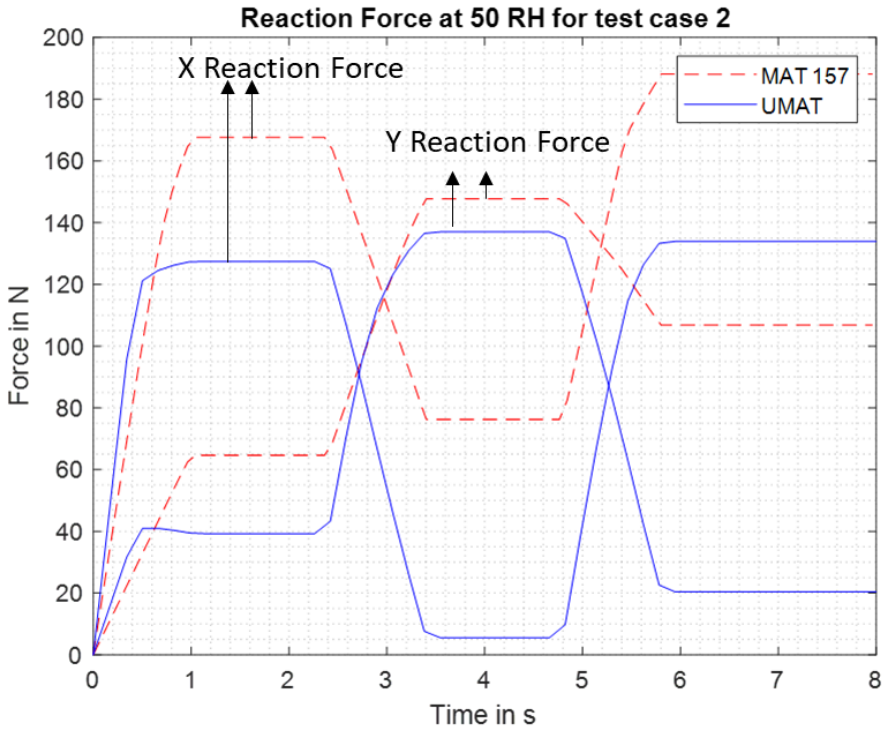

Figure B.10 Reaction forces at clamps at 50 % RH for test case 2

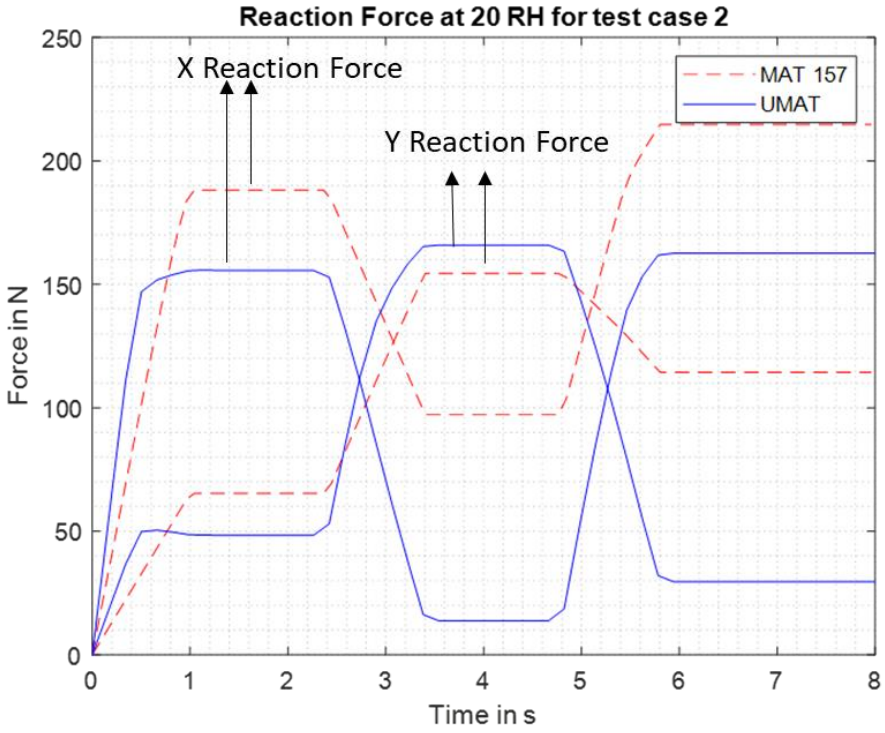

Figure B.11 Reaction forces at clamps at 20 % RH for test case 2

B.4 DISCUSSION – BIAXIAL TESTING

Updating Flow stress:

The flow stress updating mentioned in the section works very well for uniaxial simulation. The same does not apply to biaxial specimens because the plastic strain accumulated in a biaxial loading (multi-axial loading) condition cannot be used to update the uniaxial flow stress. Using the same procedure, the solution did not converge in the biaxial simulations. This was the reason to consider ideal plasticity for the UMAT in biaxial simulations.

This problem can be solved by defining the flow stress (or hardening modulus) in every direction as a function of plastic strain in that respective direction. The plastic strain evaluation might be trickier but can be identified through careful processing of uniaxial data.

The other way would be identifying the flow stress through a simple relationship that is identified from Figure B.12.

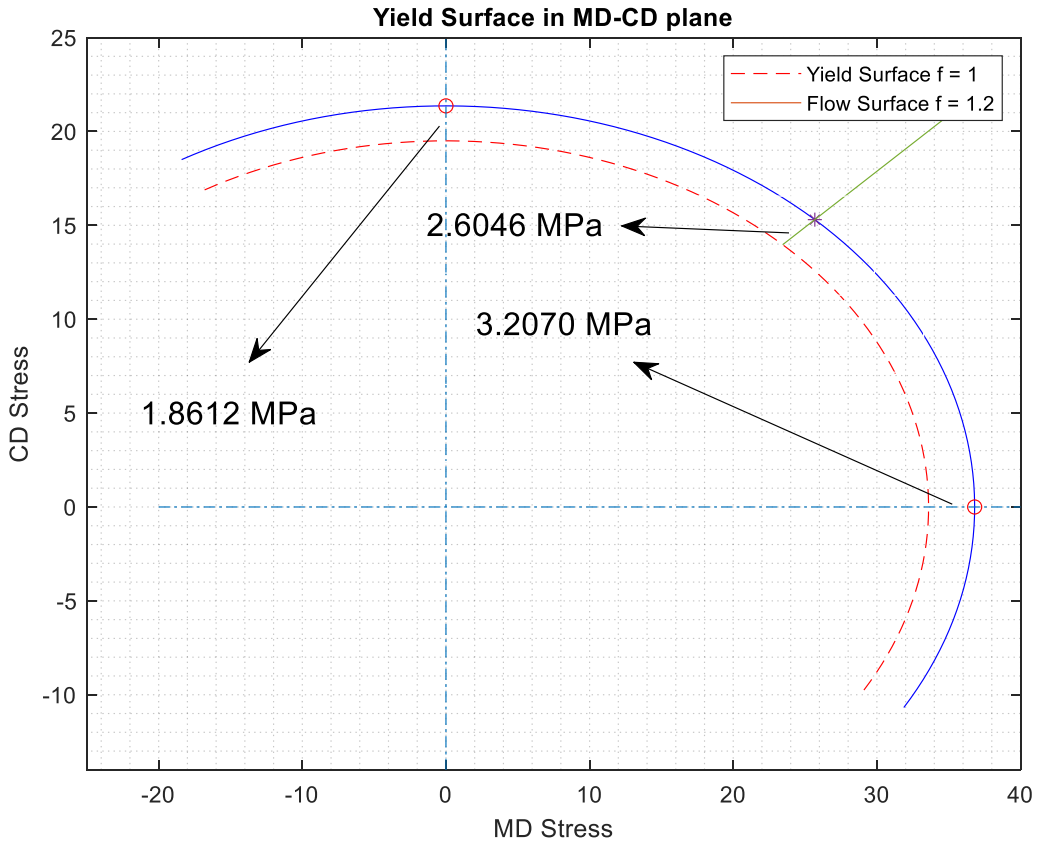

Figure B.12 Identification of flow stress for the next iteration

From the final in-plane solution, $(\sigma_{MD}, \sigma_{CD}, \sigma_{MDCD})$, it is known that

$$\left(\frac{\sigma_{MD}}{\sigma_{MD}^{y}}\right)^2 + \left(\frac{\sigma_{CD}}{\sigma_{CD}^{y}}\right)^2 + \left(\frac{\sigma_{MDCD}}{\sigma_{MDCD}^{y}}\right)^2 = 1.2$$

Where $\sigma_{MD}^{y}, \sigma_{CD}^{y}, \sigma_{MDCD}^{y}$ are the yield stresses for MD, CD, and in-plane shear stress, respectively. The uniaxial flow stresses MD and CD can be computed as

$$f = 1.2 = \left(\frac{\sigma_{MD}}{\sigma_{MD}^{y}}\right)^2 + \left(\frac{\sigma_{CD}}{\sigma_{CD}^{y}}\right)^2 + \left(\frac{\sigma_{MDCD}}{\sigma_{MDCD}^{y}}\right)^2 = \left(\frac{\sigma_{MD}^{f}}{\sigma_{MD}^{y}}\right)^2 = \left(\frac{\sigma_{CD}^{f}}{\sigma_{CD}^{y}}\right)^2$$

$$\Rightarrow \frac{\sigma_{MD}^{f}}{\sigma_{MD}^{y}} = \frac{\sigma_{CD}^{f}}{\sigma_{CD}^{y}} = \sqrt{\left(\frac{\sigma_{MD}}{\sigma_{MD}^{y}}\right)^2 + \left(\frac{\sigma_{CD}}{\sigma_{CD}^{y}}\right)^2 + \left(\frac{\sigma_{MDCD}}{\sigma_{MDCD}^{y}}\right)^2}$$

Biaxial Results:

The material models considered MAT 157 (normalized isotropic hardening) and UMAT (with ideal plasticity) in the simulations vary a lot. This is seen in all of the results for both test cases in the biaxial sample.

Test case 1: The displacements for point P follow the same pattern but differ in the value. The difference in displacements at humidity levels of 20, 50, 70 % RH seems to be small, but they vary a lot at 90 % RH. This difference can be attributed to the different hardening conditions in material models. The reaction force also seems to follow the same pattern for both material models but there is a difference in values. The difference in the reaction forces is very small at humidity levels of 20, 50, 70 % RH. The difference is quite noticeable at 90 % RH. The difference arises due to different modeling considerations in the material models. The large difference between displacements and reaction force in 90 % RH simulations can be attributed to poor uniaxial estimation.

Test case 2: The displacement results for both material models at all humidity levels of 20, 50, 70, 90 % RH are not comparable with each other. This can be attributed to the difference in material modeling and poor estimation of yield stress for the in-plane shear stress. The difference in reaction forces is less and they seem to follow the same pattern at humidity levels of 20, 50,70 % RH. The reaction forces at 90 % RH are nowhere comparable and are similar to test case 1.

APPENDIX C MATERIAL CARD DEFINITION

The material card definitions for MAT 157 in an MD sample and CD sample are shown respectively in Figure C.1 and Figure C.2 . The material parameters defined in this material card are $Q_{r1}, C_{r1}, Q_{r2}, C_{r2}$ *and* C_{11} *to* C_{66}. The parameters $Q_{r1}, C_{r1}, Q_{r2}, C_{r2}$ are defined in Chapter 4. The other parameters C_{11} *to* C_{66} are the stiffness matrix defined in section 3.1.1. The only difference in MD and CD material cards is that the yield stress and hardening parameters. The other material parameter is *'ro'*: the material density and *'mid'* is material identification.

```
*MAT_ANISOTROPIC_ELASTIC_PLASTIC_TITLE
anisotropic_isotropic_hardening
$#      mid        ro      sigy      lcss       qr1       cr1       qr2       cr2
         1  26.87600E-7     33.60         0   2195349     0.001       0.0       0.0
$#      c11       c12       c13       c14       c15       c16       c22       c23
    6454.8    1342.3   11.8733       0.0       0.0       0.0    3249.5   10.1499
$#      c24       c25       c26       c33       c34       c35       c36       c44
       0.0       0.0       0.0  192.0417       0.0       0.0       0.0    2720.9
$#      c45       c46       c55       c56       c66       r00       r45       r90
       0.0       0.0      92.0       0.0      92.0       0.0       0.0       0.0
$#      s11       s22       s33       s12      aopt        vp         -      macf
       0.0       0.0       0.0       0.0       0.0       0.0       0.0         1
$#       xp        yp        zp        a1        a2        a3                extra
       0.0       0.0       0.0       0.0       0.0       0.0       0.0       0.0
$#       v1        v2        v3        d1        d2        d3      beta      ihis
       0.0       0.0       0.0       0.0       0.0       0.0       0.0       0.0
```

Figure C.1 Material card data for MAT 157 at 50 RH – MD sample

```
*MAT_ANISOTROPIC_ELASTIC_PLASTIC_TITLE
anisotropic_isotropic_hardening
$#      mid        ro      sigy      lcss       qr1       cr1       qr2       cr2
         1  26.87600E-7     19.60         0    333707     0.001       0.0       0.0
$#      c11       c12       c13       c14       c15       c16       c22       c23
    6454.8    1342.3   11.8733       0.0       0.0       0.0    3249.5   10.1499
$#      c24       c25       c26       c33       c34       c35       c36       c44
       0.0       0.0       0.0  192.0417       0.0       0.0       0.0    2720.9
$#      c45       c46       c55       c56       c66       r00       r45       r90
       0.0       0.0      92.0       0.0      92.0       0.0       0.0       0.0
$#      s11       s22       s33       s12      aopt        vp         -      macf
       0.0       0.0       0.0       0.0       0.0       0.0       0.0         1
$#       xp        yp        zp        a1        a2        a3                extra
       0.0       0.0       0.0       0.0       0.0       0.0       0.0       0.0
$#       v1        v2        v3        d1        d2        d3      beta      ihis
       0.0       0.0       0.0       0.0       0.0       0.0       0.0       0.0
```

Figure C.2 Material card data for MAT 157 at 50 RH – CD sample

The material card for the UMAT is shown in Figure C.3. The same material card can be used for both MD and CD samples and the same in even biaxial testing. The *'mt'* is the material subroutine number called. In this case, it is 41. The '*lmc*' is the length of the array of material constants and it is 16 in this card. '*nhv*' are the number of history variables stored. '*iortho*' is a Boolean operator to define the orthotropic behavior of the material. Similarly, '*ivect*' is the Boolean operator for the vectorized subroutine implementation. '*ibulk*' and '*ig*' are the locations of bulk modulus and shear modulus in the '*lmc*' array.

The '*lmc*' array is in two rows defined from '*p1 -p8*'. The first row corresponds to the first 8 entries in the array and the second row corresponds to the next 8 entries in the array. The

material constants array is defined as '*cm*' in the subroutine. The code snippet which defines every parameter is shown in Figure C.4.

```
*MAT_USER_DEFINED_MATERIAL_MODELS_TITLE
User Defined Material
$#     mid        ro        mt       lmc       nhv    iortho     ibulk        ig
         1  36.87600E-7        41        16        20         1         1         7
$#   ivect     ifail    itherm    ihyper      ieos      lmca    unused    unused
         1         0         0         0         0         0
$#    aopt      mafc        xp        yp        zp        a1        a2        a3
       0.0       1.0       0.0       0.0       0.0       0.0       0.0       0.0
$#      v1        v2        v3        d1        d2        d3      beta     ievts
       0.0       0.0       0.0       0.0       0.0       0.0       0.0         0
$#      p1        p2        p3        p4        p5        p6        p7        p8
    5900.0    2970.0    190.15    0.2079      0.04      0.04   2720.93      92.0
$#      p1        p2        p3        p4        p5        p6        p7        p8
      92.0      33.6      19.6      27.0  2195.349  333.7079   1.08108   6454.81
```

Figure C.3 Material card data for UMAT at 50 RH

```
cm(1)=E_a; Stiffness in MD
cm(2)=E_b ; stiffness in CD
cm(3)=E_c; Stiffness in ZD
cm(4)=v_ba; possions ratio in MDCD
cm(5) =v_ca ; possions ratio in MDZD
cm(6)=v_cb; possions ratio in MDCD
cm(7) =g_ab ; shear modulus in MDCD
all at 50% RH
cm(8)= gbc ; shear modulus in CDZD
cm(9) = gca ; shear modulus in ZDMD
cm(10) =s_MD ; tensile yield stress in MD
cm(11) = s_CD; tesile yield stress in CD
cm(12) = s_MDCD; shear yield stress in MDCD
cm(13) = H_MD ; Hardening in MD
cm(14) = H_CD; Hardening in CD
cm(15) = m_r ; normalized moisture ratio
cm(16) = C 11 ; First Diagonal term in element stiffness
```

Figure C.4 Code snippet defining material parameters in the local coordinate system

Definition of bulk modulus and shear modulus:

The bulk modulus and shear modulus are required for transmitting boundaries, contact interfaces, rigid body constraints, and time step calculations (refer (Livermore Software Technology Corporation (LSTC), 2019) for more information). For an isotropic material, bulk and shear modulus can be computed easily from other parameters like stiffness and poison's ratio. This is not the same for orthotropic material since it has three shear moduli, and the definition of bulk modulus definition is not straightforward.

The shear modulus and bulk modulus needed for the necessary computation in an orthotropic material is defined as

Shear modulus – $\max(G_{xy}, G_{yz}, G_{xz})$ – generally, it is the in-plane shear modulus

Bulk Modulus – $\max(C_{11}, C_{22}, C_{33})$ – maximum of the diagonal elements in the stiffness matrix.

TRITA SCI-GRU 2020:323